Part I
Integration of Heat Transfer and Chemical Reactions

1
Enhancing Productivity and Thermal Efficiency of High-Temperature Endothermic Processes in Heat-Integrated Fixed-Bed Reactors

Grigorios Kolios, Achim Gritsch, Bernd Glöckler and Gerhart Eigenberger

Abstract

High-temperature endothermic processes (e.g., reforming of hydrocarbons) are widely utilized in the production of basic chemicals and fuels from fossil feedstocks. These processes require large amounts of heat at temperatures up to 1000 °C. In conventional solutions, only about half of the high-temperature heat supplied is transferred into the endothermic reaction. Emerging applications such as decentralized hydrogen production for residential and mobile power generation require considerable improvement in specific productivity and thermal efficiency. Thus, this topic is currently the subject of exciting research activities in industry and academia. This chapter provides an introduction to the fundamentals of heat-integrated processes, an overview on conceptual trends in process and apparatus design, and an analysis of the state of the art, with emphasis on steam reforming of methane.

1.1
Introduction

Endothermic high-temperature processes stand at the beginning of the chemical production chain – for example, syngas is produced mainly through steam reforming of naphtha or natural gas, ethylene and propylene through steam cracking, and styrene through dehydrogenation of ethylbenzene. These processes are usually conducted in large furnaces and belong naturally to the largest fuel consumers. At the same time, they have a significant heat surplus since typically only about 50 % of the heat generated is consumed by the endothermic reaction. In large product- and energy-integrated chemical sites, waste heat can be utilized in subsequent processes. However, rigid thermal coupling throughout the plant imposes constraints regarding the heat balance of individual processes and requires a considerable overhead in order to adjust plant-wide optimal operating conditions. This problem could be significantly relaxed by reducing the surplus of the heat exporters. This is one strong incentive for enhancing the thermal efficiency of endothermic high-temperature processes.

Integrated Chemical Processes. Edited by K. Sundmacher, A. Kienle and A. Seidel-Morgenstern

ISBN 3-527-30831-8

Two emerging trends endorse the concept of heat-integrated processes: first, the production of basic chemicals is moved close to oil and gas wells where crude oil or natural gas is processed in large stand-alone units [1]. Second, fuel cell systems require on-site and on-demand hydrogen production from primary fuels (i.e., natural gas, liquid hydrocarbons or alcohols) [2]. Net heat generation in these processes is equivalent to raw material and energy loss, and is therefore undesirable.

While many publications in the field of heat-integrated processes focus on specific processes such as dehydrogenation of paraffins or hydrogen production [3–5], this chapter is more focused on general conceptual trends in process and apparatus design.

1.2 Heat-Integrated Processes for Endothermic Reactions

The intended purpose of heat-integrated processes for endothermic reactions is illustrated by the example of methane steam reforming for hydrogen generation, which is of high practical relevance [6] and features typical characteristics of the considered process class. The reaction is given by the following stoichiometric equation:

$$CH_4 + H_2O \leftrightarrow 3H_2 + CO \quad ; \quad \Delta H_R\left(950^{\circ}C, 20bar\right) = 235\,{}^{kJ}\!/_{mol}$$

Figure 1.1 shows the heat fluxes required at different process stages for the generation of H_2 equivalent to 1 kW combustion enthalpy based on the lower heating value of hydrogen (LHV, H_2). Typically, the feed composition of the technical process corresponds to a steam-to-carbon molar ratio of S:C = 3:1. The reaction temperature is determined by chemical equilibrium. The heat consumption of the steam-reforming reaction is equivalent to around 30 % of the lower heating value of the produced hydrogen. The amount of heat required for heating the gaseous feed to reaction tem-

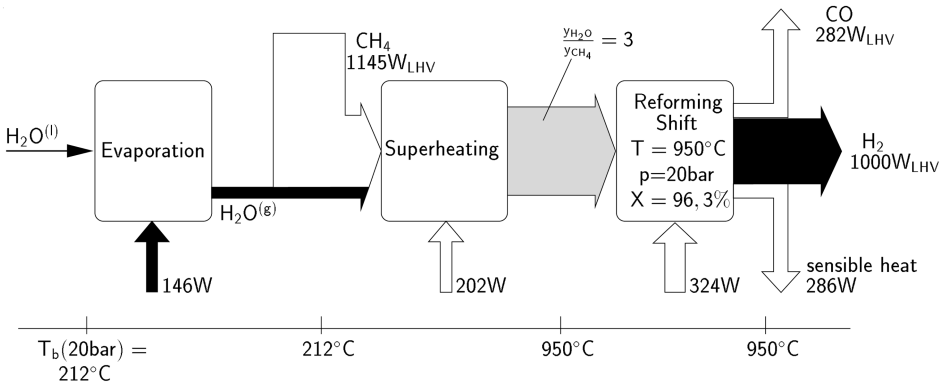

Fig. 1.1. Heat fluxes for hydrogen generation by steam reforming of methane.

perature corresponds to almost 20 % of the heat of combustion. On the other hand, a considerable amount of sensible heat contained in the product stream is usable for feed preheating.

Heat-integrated processes comprise two additional functions besides the main (endothermic) reaction: process heat generation and heat recovery. As shown above, both aspects are equally important, since the heat of reaction and the heat required for feed preheating are in the same range. Figure 1.2 shows, schematically, two different configurations of heat-integrated processes. The process comprises two thermally interconnected reaction stages for the endothermic reaction and for the combustion. Heat exchangers on both sides perform heat recovery by coupling feed preheating with product cooling. In the first configuration (Fig. 1.2(a)) the endothermic reaction mixture and the combustion gas flow countercurrently through all process stages such that the hot effluent from the exothermic reaction is used to heat up the cold feed for the endothermic reaction, and vice versa. In the second configuration (Fig. 1.2(b)), thermal contact between the two process streams is limited to the reaction stage, while heat recovery is separated between the flows of the exothermic and the endothermic reactions.

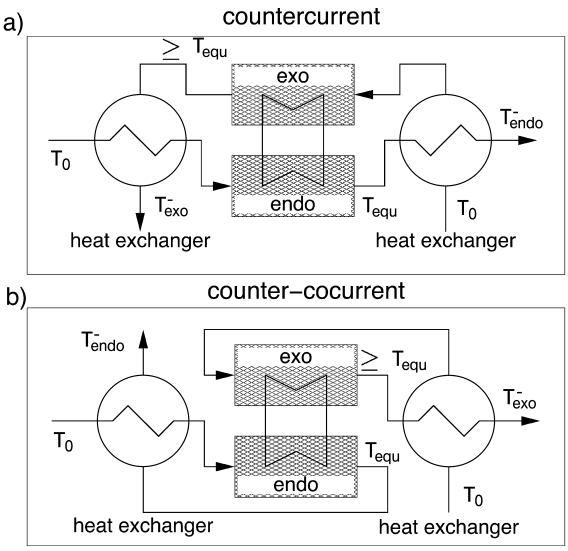

Fig. 1.2. Schematic flow configurations of heat-integrated processes for coupling endothermic and exothermic reactions. (a) Countercurrent flow of process streams. (b) Cocurrent flow of the process streams in the reactor stages and heat recovery in separate circuits.

1.2.1 Optimality Conditions

1.2.1.1 Efficiency of Heat Recovery

Analysis of the overall heat balance yields basic conditions for optimal heat recovery. The optimizing condition is minimization of heat loss. The feed temperatures of the two process streams, T_0, and the outlet temperature of the endothermic stage, T_{equ}, are fixed (Fig. 1.2) where T_{equ} is the temperature required for the desired conversion under equilibrium conditions. Obviously, T_{equ} is also a lower limit of the temperature in the combustion stage. The performance of the heat exchangers is given by the mean heat transfer coefficient k_h and the heat exchange area A. Both heat exchangers are assumed to be identical. The mass flow rate of the endothermic mixture and the combustion gas is $\dot{M}_{endo}$ and $\dot{M}_{exo}$, respectively. Crucial parameters for the efficiency of heat recovery are the heat capacity ratio of the process streams (h) and the number of transfer units of the heat exchangers (NTU):

$$h = \frac{\left(\dot{M} \quad c_p\right)_{endo}}{\left(\dot{M} \quad c_p\right)_{exo}} \tag{1}$$

$$NTU_{endo} = \frac{k_h \quad A}{\left(\dot{M} \quad c_p\right)_{endo}} \; ; \; NTU_{exo} = \frac{k_h \quad A}{\left(\dot{M} \quad c_p\right)_{exo}} = \frac{NTU_{endo}}{h} \tag{2}$$

Taking the amount of heat required for bridging the temperature gap ($T_{equ} - T_0$) for the endothermic mixture as a reference, the normalized heat loss is given by the following expression:

$$loss_{norm} = \frac{\left(\bar{T}_{endo} - T_0\right) + h \quad \left(\bar{T}_{exo} - T_0\right)}{T_{equ} - T_0} \tag{3}$$

A value of $loss_{norm} = 1$ indicates that the total heat loss via the exit streams of the exothermic and the endothermic stage is equal to the amount of heat required to heat up the feed of the endothermic stage about $\Delta T = T_{equ} - T_0$. $loss_{norm}$ can be expressed explicitly as a function of h and NTU_{endo} taking into account the theory of ideal countercurrent heat exchangers [7].

At this point, a distinction is required between the two configurations shown in Fig. 1.2. In the countercurrent configuration the heat capacity fluxes of the heat exchanging streams are generally differing, whereas in the counter-cocurrent configuration they are equal to each other. Hence, we obtain:

$$loss_{norm} = (h-1)\frac{h + e^{\frac{h-1}{h} NTU_{endo}}}{h - e^{-\frac{h-1}{h} NTU_{endo}}} \quad \text{for countercurrent configuration} \tag{4}$$

$$loss_{norm} = \frac{1}{NTU_{endo}+1} + \frac{h^2}{NTU_{endo}+h} \quad \text{for counter-cocurrent configuration} \quad (5)$$

Figure 1.3 illustrates the dependence of $loss_{norm}$ on h and NTU_{endo} for both configurations.

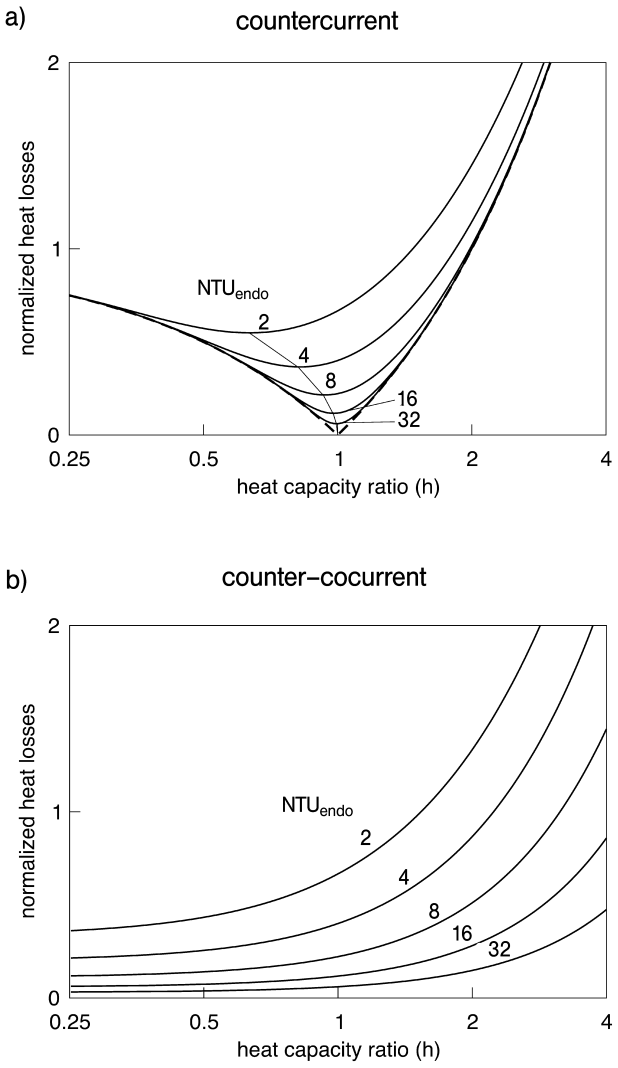

Fig. 1.3. The effect of heat exchanger performance, NTU, and heat capacity ratio, h, on the normalized heat loss for heat-integrated processes in (a) countercurrent and (b) counter-cocurrent flow configuration.

For the countercurrent configuration the optimal heat capacity ratio converges asymptotically to $h = 1$ with increasing NTU values. Even for an ideal heat exchanger (NTU $\rightarrow \infty$), small deviations from the optimal heat capacity ratio cause significant heat losses. On the other hand, heat losses could be minimized with decreasing heat capacity ratio and increasing NTU values for the counter-cocurrent configuration. In this case the heat recovery becomes complete for an ideal heat exchanger (NTU $\rightarrow \infty$) independent of the heat capacity ratio h.

1.2.1.2 **Temperature Control**

Conventional steam reformers are furnaces containing tubes filled with reforming catalyst. Radiation burners, which are usually installed at the top and the bottom of the furnace, generate the process heat (Fig. 1.4(a)). Figure 1.4(b) shows a schematic lateral temperature profile inside a single reformer tube.

Clearly, in the considered high-temperature processes the process conditions are defined mainly through the thermal stability of the tubes. A considerable temperature difference across the tube wall is required as the driving force for the heat supply to the reforming reaction. The main heat transfer resistances occur at the inner and outer surface of the tube wall.

The impact of heat transfer limitations is illustrated with a generic example describing a best-case scenario (Fig. 1.5). The allowed maximum temperature of the reformer tube is assumed at 950 °C. Hence, the wall temperature and inlet temperature of the reaction gas are set to 950 °C. The reforming reaction is assumed to be instantaneous – that is, at each axial position conversion is set equal to the equilibrium conversion at the respective temperature $X_{equ}(T)$. Dissipative effects (i.e.,

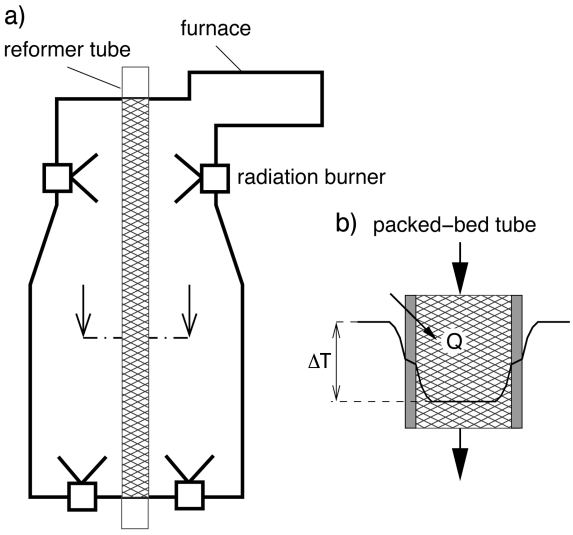

Fig. 1.4. Simplified scheme of an industrial steam reformer furnace. (a) Furnace with radiation burners adapted from [6]. (b) Lateral temperature profile inside a single reformer tube.

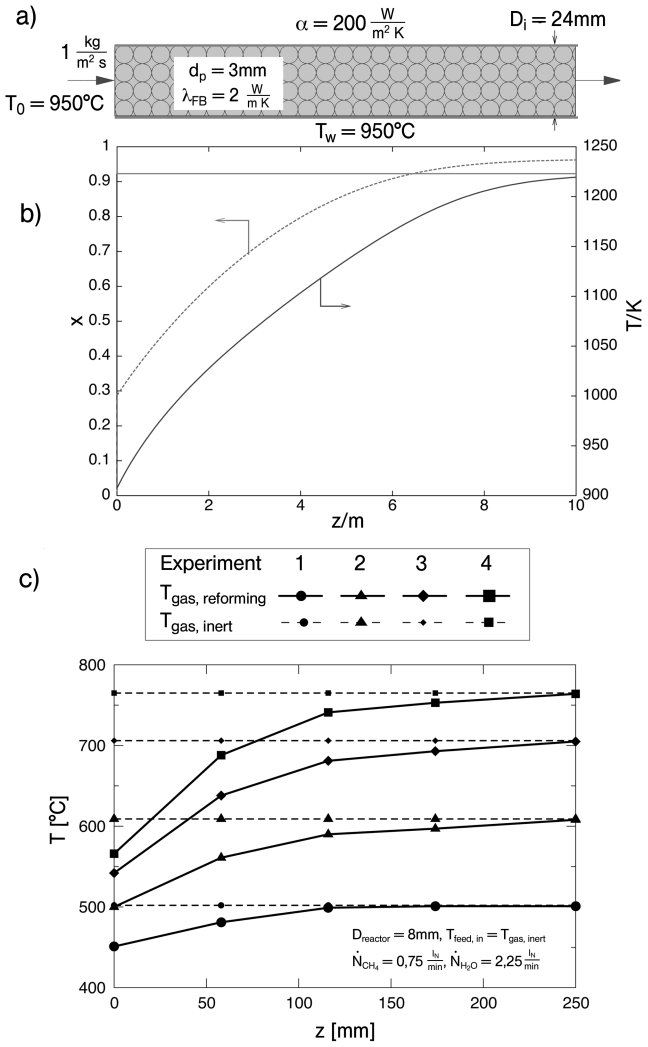

Fig. 1.5. Effect of heat transfer limitation in industrial steam reformers. (a) Scheme of a single catalytic fixed-bed reformer tube with typical heat transfer and operating parameters. (b) Computed temperature profile (solid line) and equilibrium conversion profile (dashed line) in flow direction for a tubular reformer. (c) Measured fixed-bed temperature profiles at different wall temperatures in a tubular reformer (D_i = 8 mm) filled with spherical catalyst pellets (d_p = 1.5 mm).

diffusion and heat conduction) are neglected in the axial direction. Finally, we assume a uniform fixed-bed temperature in radial direction. Based on this model the axial temperature profile of the fixed bed is given by the following relationship [8]:

$$\dot{M} c_p \left(1 + \left|\Delta T_{ad}\right| \frac{dX_{equ}}{dT}\right) \frac{dT_c}{dz} = \alpha_w \frac{4}{D_i}\left(T_w - T_c\right) \tag{6}$$

Figure 1.5(b) shows the axial temperature profile of the packing for a favorable heat transfer coefficient at the tube wall of $\alpha_w = 200\ W/m^2/K$ and a small tube diameter of $D_i = 25mm$. The temperature at the inlet cross-section drops immediately to the equilibrium value corresponding to the feed conditions. Further downstream, the temperature increases gradually and approaches asymptotically the wall temperature. A reactor length of approximately 10 m would be necessary in order to reach an equilibrium conversion of 95 %. According to this result, heat transfer limitations between the catalyst packing and the heating tube wall result in poor catalyst utilization. This has been verified experimentally with a laboratory-scale reactor of 8 mm inner diameter (Fig. 1.5(c)). Despite the significantly larger specific heat transfer area of this tube, a temperature drop of up to 200 K has been observed at the entrance to the catalytic bed. Similar behavior – although not especially extreme – is observed with endothermic reactions running under milder conditions. For example, during styrene synthesis in a 2.5-cm tube a temperature difference up to 30 K has been measured between the reactor wall and its center [9]. This heat transfer limitation could be overcome by depositing the catalyst directly on the surface of the tube wall – that is, by using a wall reactor concept. Charlesworth et al. [10] estimated that such a reactor would be two orders of magnitude smaller than a conventional steam reformer.

The above considerations indicate that, independent of implementation details, the space–time yield of endothermic reactions could be significantly enhanced by shifting the reaction site to the heat-exchanging surfaces. This intention has led to the production of a large variety of multifunctional reactor concepts for coupling endothermic and exothermic reactions. In the following section the state of the art in this area will be discussed for selected examples.

1.3 Multifunctional Reactor Concepts

Figure 1.6 contains a classification of multifunctional reactor concepts with integrated heat recovery for coupling endothermic and exothermic reactions [11]. Coupling of methane steam reforming with methane combustion is displayed as a representative example. Equivalent processes can be created based on recuperative heat exchange in a stationary operation mode (left column) or based on regenerative heat exchange in a cyclic operation mode (right column).

The simultaneous mode is the simplest configuration where the feed streams of the endothermic mixture and the combustion gas are mixed and react

simultaneously in the same volume. The amount of oxygen is adjusted to generate sufficient excess heat, in order to compensate non-idealities of heat recovery. The simultaneous mode has been widely applied in technical processes, for example, in autothermal reforming or in oxidative dehydrogenation processes. However, mixing of the process streams imposes substantial constraints to the process conditions, since they must be compatible to the endothermic and to the exothermic subsystem. For example, high-pressure operation, often desirable for steam reforming, would

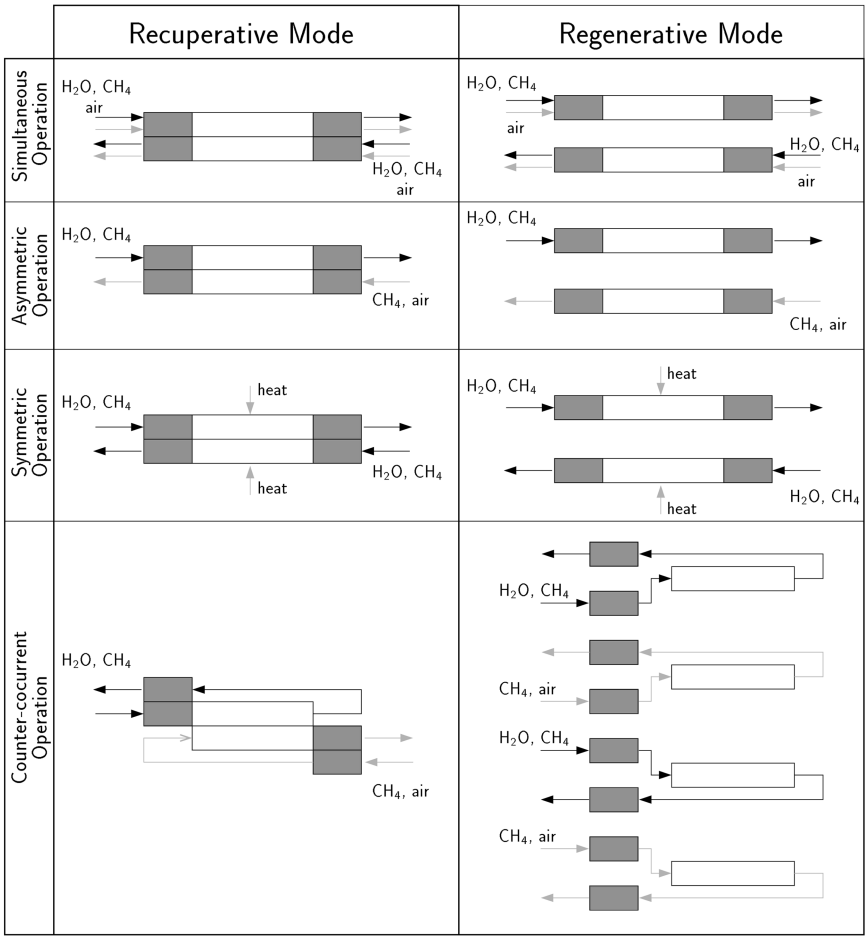

Endothermic reaction: $CH_4 + H_2O \rightleftharpoons 3H_2 + CO$
Exothermic reaction: $CH_4 + 2O_2 \rightarrow 2H_2O + CO_2$

Fig. 1.6. Schematic classification of heat-integrated concepts for the representative example of coupling methane steam reforming and methane combustion.

require pressurization of the combustion air. Finally, dilution of the product by the exhaust gas stream complicates subsequent purification steps.

In the asymmetric mode of operation the endothermic and exothermic reactions take place separately either in different compartments (recuperative mode) or at different time intervals (regenerative mode). The attractiveness of the asymmetric mode is related to the fact that the separation of the process streams allows an individual tuning of the operating conditions for the endothermic and the exothermic subsystem.

The symmetric mode aims at combining the advantages of the simultaneous and the asymmetric mode: only the endothermic reaction takes place in the main reactor. The process heat is added through a hot, inert side stream (e.g., the effluent gas of an external combustion chamber). The side stream can be distributed along the reactor in order to adjust a specific temperature profile.

The counter-cocurrent concept features a modular design: it provides separate heat exchanger loops for heat recovery within the endothermic mixture and the combustion gas. Cocurrent flow of exothermic and endothermic process streams is principally favorable with respect to the controllability of heat release.

As indicated by this schematic representation, different configurations vary with respect to the degree of coupling between the process streams. The strongest coupling occurs in the simultaneous mode, where chemical and thermal interaction occurs between the process streams. In contrast to this, the counter-cocurrent concept features only thermal interaction between the process streams localized in the reactor stage.

As stated earlier in Section 1.2.1.1, equality of the heat capacity fluxes in the heat recovery sections is a crucial condition for efficient heat recovery. This condition is inherently fulfilled by the simultaneous and the counter-cocurrent concept. In the asymmetric concept the flow rates of the process streams must be adjusted accordingly. The requirement of equal heat capacity fluxes cannot be fulfilled in the symmetric concept due to the continuous side stream addition. However, besides these structural properties the design details are decisive for their specific performance and efficiency of individual solutions.

1.3.1 Regenerative Processes

Surprisingly, the majority of advanced heat-integrated reactor concepts employ a cyclic mode of operation with regenerative heat exchange. They have been proposed mainly for syngas and olefin production. Their potential field of application is in large chemical and petrochemical processes, where a compact reactor could replace a complex network of reactors and heat exchangers. The following survey reflects the classification introduced in Fig. 1.6.

1.3.1.1 **Simultaneous Mode**

A pioneering report on the simultaneous concept with integrated heat recovery proposes a reverse-flow mode of operation for syngas production from natural gas [12]. The process is implemented in an adiabatic fixed-bed reactor with inert end zones and a catalytically active section in the middle. The experiments confirm the feasibility of the concept. The results of this investigation, together with those of subsequent studies [13, 14], indicate that local excess temperatures up to 1500 °C are the major problem of this concept. One reason for this is the tendency for the reaction zones of combustion and reforming to separate from each other. Due to a preferential adsorption of oxygen on the catalyst surface, total oxidation of hydrocarbons is favored [15]. Steam reforming and the water-gas-shift reaction take off after complete depletion of oxygen. Additionally, ignition of homogeneous combustion is unavoidable if the temperature exceeds 600 °C. Coke formation in the heat-exchange zones has been identified as an additional reason for the temperature runaway. De Groote et al. [13] show that the major source of coke in the upstream section is methane cracking and the Boudouard equilibrium in the downstream section. The sudden ignition of accumulated coke may lead to extreme local temperature peaks.

1.3.1.2 **Asymmetric Mode**

The CATOFIN process developed by ABB-Lummus for dehydrogenation of C3–C4 paraffins [16, 17] can be considered as the prototype process of coupling endothermic and exothermic reactions. Figure 1.7 shows the process scheme in schematic form. Each cycle includes the production phase and two regeneration steps. The heat consumption of the endothermic reaction during the production phase is taken from the heat stored in the fixed bed. The thermal reservoir is restored by a superheated air purge during the second phase. In addition to convective heating, heat is generated through the combustion of carbonaceous deposits. Finally, hydrogen is passed over the fixed bed in order to convert the catalyst back to its reduced, active form, and this produces additional heat. A similar concept has been proposed for

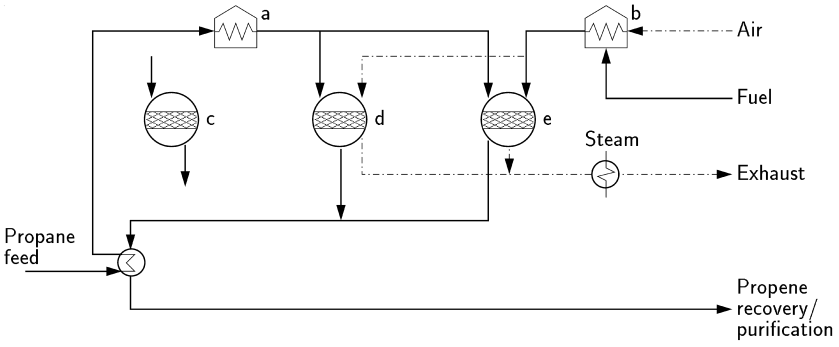

Fig. 1.7. CATOFIN process: dehydrogenation of propane adapted from Ullmann [54]. (a) charge heater; (b) air heater; (c) purge step; (d) production step; (e) regeneration step.

styrene synthesis [18]. The attraction of this concept results from the simplicity of the reactor – a simple adiabatic fixed-bed type – and the process-integrated regeneration of the catalyst – that is, the removal of carbonaceous deposits. Both, cocurrent flow and countercurrent flow have been investigated. The authors concluded that the reverse-flow mode is superior with regard to selectivity because the endothermic reaction runs along an increasing temperature profile. However, at a low air-to-hydrocarbon ratio the yield of the cocurrent-flow mode is higher than in the reverse-flow mode. This is due to a wrong-way phenomenon caused by coupling the endothermic reaction with countercurrent heat exchange.

Figure 1.8 illustrates the operating behavior of the reverse-flow CATOFIN process in the limit of equal heat capacities during reaction and regeneration cycle ($h = 1$). The inlet temperature of the regeneration gas is set approximately $|\Delta T_{ad}|$ above the inlet temperature of the endothermic reaction feed. In the periodic steady state, only two narrow zones close to both reactor ends contribute considerably to the conversion, while the major part of the fixed bed cools down to a temperature level well

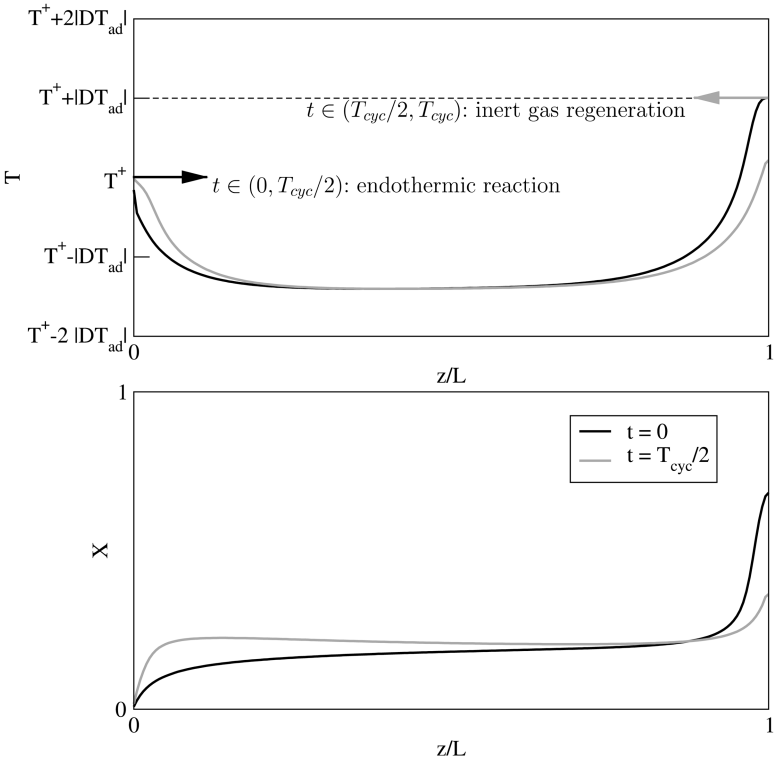

Fig. 1.8. Reverse-flow CATOFIN process at equal heat capacity fluxes during production and regeneration cycle: periodic temperature profiles (top) and conversion profiles (bottom) at the end of the endothermic semicycle ($t = t_{cyc}/2$) and the regeneration cycle ($t = 0$).

below the adiabatic temperature drop of the endothermic reaction. The accumulation of heat consumption of the endothermic reaction in the fixed bed is the reverse analogy to the accumulation of heat of weakly exothermic reactions in autothermal reactors [19]. This counter-intuitive effect indicates the complexity of coupling chemical reactions with countercurrent heat exchange.

The asymmetric reverse-flow operation mode as proposed by Levenspiel [20] is a straightforward extension of the CATOFIN process in order to integrate heat generation and heat recovery in the reactor. Its application in syngas production has been studied theoretically in a series of papers by Kulkarni and Duduković [21, 22]. This study demonstrates the feasibility of coupling methane steam reforming with methane combustion, but it also reveals the susceptibility of the process to severe overheating. Operation with preheated feed during the exothermic semicycle is proposed as a remedy.

A detailed analysis of an asymmetric process coupling styrene synthesis through dehydrogenation of ethylbenzene with combustion of hydrogen has been presented in [23]. Figure 1.9 shows typical periodic steady-state conditions of the process. One

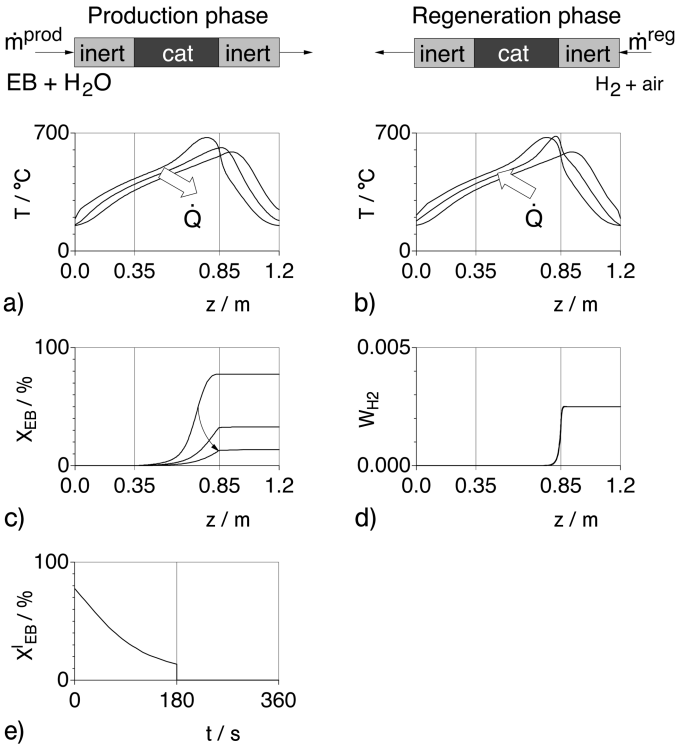

Fig. 1.9. Coupling of dehydrogenation of ethylbenzene to styrene and hydrogen combustion in a catalytic fixed-bed reverse flow reactor [9]. (a, b) Fixed-bed temperature profiles during production and regeneration cycle. (c) Ethylbenzene conversion during production cycle. (d) Hydrogen weight fraction during regeneration cycle. (e) Ethylbenzene conversion during one period.

finding of this study is the importance of structuring the fixed bed in catalytic and inert sections. In particular, a sufficient length of the right inert zone is decisive for the establishment of a sufficient temperature level in the catalytic part. However, heat release within a narrow zone at the right end of the catalytic section implies inefficient heat storage. The initial temperature profile of the endothermic semicycle enables indeed high conversion at a high selectivity, but subsequently the temperature peak is shifted into the right inert section and becomes useless.

The major conclusions from the above-described studies are consistent: in the asymmetric mode of operation the reaction zones of the exothermic and endothermic reactions inherently repel each other, leading either to an extreme maximum temperature or to poor performance. A noncontinuous heat supply and production during every other semicycle cause obviously strong fluctuations of operation. Moreover, reasonable states of operation are attainable only with an excess of gas during the exothermic semicycle. This contradicts the condition of equal heat capacities for optimal heat recovery (see Section 1.2.1.1). For example, the heat loss in the case displayed in Fig. 1.9 is equal to the heat demand of the endothermic reaction. Different strategies have been assessed with regard to their potential to reduce hotspots during the exothermic semicycle and to improve thermal efficiency.

Latent heat storage

It is clear that temperature oscillations during heating–cooling cycles depend on the fixed-bed heat capacity. Figure 1.10 shows a simplified picture of the effect of phase change on the effective heat capacity of pure substances. Considerable amounts of

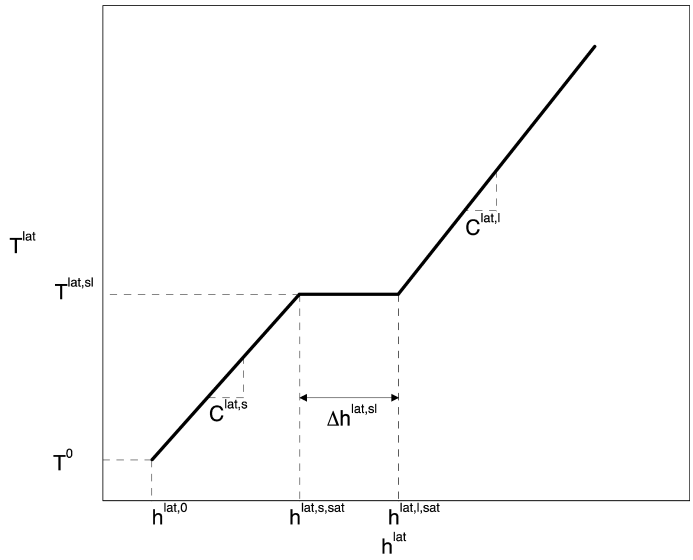

Fig. 1.10. Temperature plotted versus specific enthalpy of a pure substance undergoing phase changes (melting, solidifying).

heat can be stored at a constant temperature level at the melting point. The principle of latent heat storage is discussed in detail in Ref. [24]. Figure 1.11 illustrates the effect of adding aluminum-filled pellets to the catalytic fixed bed in the reverse-flow reactor for styrene synthesis. The melting temperature of aluminum (664 °C) is compatible with the operating temperature of the styrene catalyst. The amount of heat required for melting aluminum would be sufficient to heat-up the same amount of solid metal by approximately 400 K. In Fig. 1.11. the diagrams on the left-hand side show the conditions during the production cycle in the periodic steady

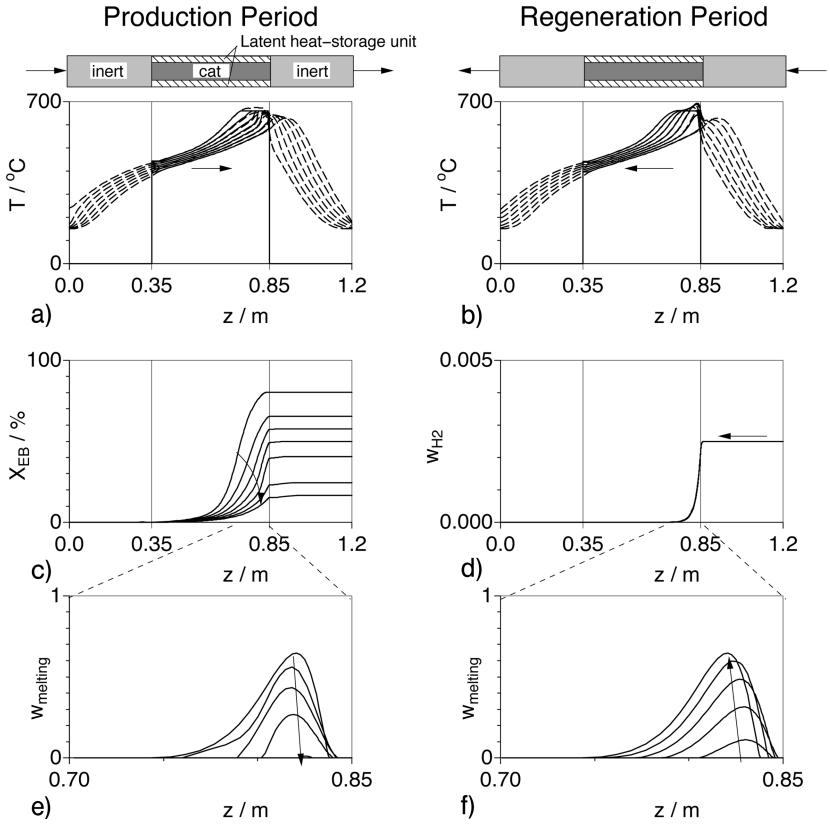

Fig. 1.11. Coupling of dehydrogenation of ethylbenzene to styrene and hydrogen combustion in a catalytic fixed-bed reverse-flow reactor with a mixed bed of catalytic pellets and aluminum powder (50:50) [23]. (a, b) Temperature profile of the latent heat storage (solid line) and of the fixed bed (dashed line) during production and regeneration periods. (c) Ethylbenzene conversion during the production cycle. (d) Hydrogen weight fraction during the regeneration cycle. (e, f) Molten fraction of the latent heat storage during production and regeneration period.

state. At the start of the endothermic semicycle, part of the aluminum has been molten and a temperature plateau has formed close to the right end of the catalytic zone. During the endothermic semicycle the fraction of molten aluminum shrinks. However, the maximum temperature remains at a constant level over a significant part of the semicycle, preventing a fast drop of the conversion profile. During the subsequent exothermic semicycle aluminum is melted again, absorbing a significant amount of the heat of combustion. It thus reduces overheating of the catalyst. Figure 1.12 shows the effect of latent heat storage on maximum temperature and conversion during a cycle in the periodic steady state. It becomes clear that the installation of heat storage has a beneficial effect on reactor performance, but it does not completely solve the problem of conversion fluctuations and suboptimal heat recovery. The major problem remains – the heat of combustion is stored within a narrow zone close to the right boundary of the catalytic section. It travels during the production phase into the inert section and becomes useless for dehydrogenation reaction.

Distributed heat release

The concepts discussed so far indicate that the major challenge in asymmetric operation is correct adjustment of the loci of heat release and heat consumption. A reactor concept aiming at an optimum distribution of the process heat has been proposed [25, 26] for coupling methane steam reforming and methane combustion. The primary task in this context is to define a favorable initial state and to assess the distribution of heat extraction from the fixed bed during the endothermic semicycle. An optimal initial state features cold ends and an extended temperature plateau in the catalytic part of the fixed bed. The downstream heat transfer zone is inert, in order to avoid any back-reaction (Fig. 1.13).

Taking into account the fact that methane steam reforming is a rapid reaction and that the local conversion is determined mainly by the catalyst temperature ($X_{ref} = X_{ref}(T)$), the evolution of the temperature profile can be estimated through a simplified procedure based on geometric considerations. It can be shown, that

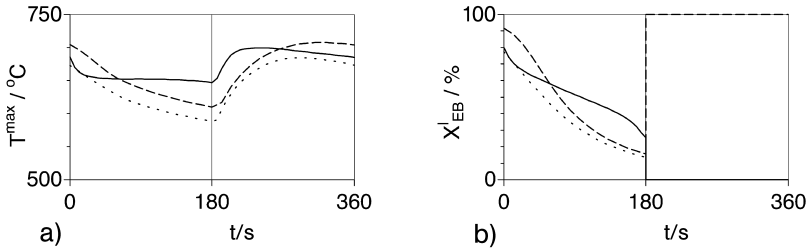

Fig. 1.12. Maximum temperature (a) and ethylbenzene conversion (b) during one production cycle for a fixed bed of uniform heat capacity (dotted line), for a structured fixed-bed with inert end sections of higher heat capacity (dashed line), and for latent heat storage inside the catalytic section (solid line) [9].

equilibrium-limited endothermic reactions lead to a sharp, traveling heat transfer zone if cold feed enters a uniformly preheated catalytic fixed bed [25]. The heat transfer zone and the reaction zone can therefore be approximated by step functions propagating through the fixed bed in flow direction. The heat transfer zones at the left and the right end of the profile propagate with the velocity of a thermal wave, w_{therm}, which depends on the heat capacity flux of the gas stream and the heat capacity of the solid phase:

$$w_{therm} = \frac{\left(\dot{m} \cdot c_p\right)_g}{\rho c} = \frac{v^0 \left(\rho \cdot c_p\right)_g}{\rho c} \tag{7}$$

In the reaction zone, superposition of convective cooling and heat consumption through the endothermic reaction leads to an accelerated cooling of the fixed bed. The ratio of the propagation velocity of the reaction front (w_{endo}) and the thermal front can be estimated as follows:

$$\frac{w_{endo}}{w_{therm}} \approx 1 + \left|\Delta T_{ad}\right| \frac{X_{ref}\left(T_{\max}\right) - X_{ref}\left(T_{low}\right)}{T_{\max} - T_{low}} \tag{8}$$

For the example of methane steam reforming, Eq. (8) yields an acceleration factor of 4. Accordingly, the axial displacement of the reaction zone is a multiple of the axial displacement of thermal fronts. The difference of the axial displacement between the reaction front and the thermal front determines the axial profile of heat demand during the subsequent exothermic semicycle. Efficient heat recovery requires equal heat capacities of the process streams during both semicycles. The initial state can be restored by discrete heat sources distributed at equal distances along the catalytic part of the reactor. Each point source initiates a thermal wave that covers the distance to the next heating point (Fig. 1.13, right). This concept features

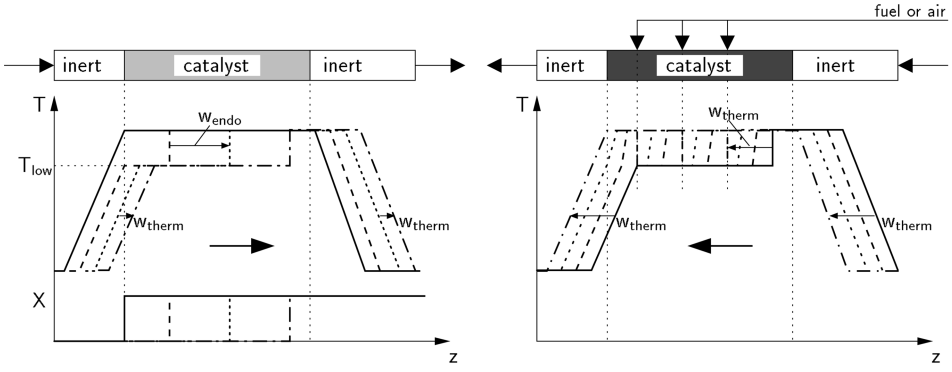

Fig. 1.13. Schematic picture of the evolution of temperature profiles in a reverse-flow reactor with distributed side feed during production (left) and regeneration cycles (right) [25].

optimal characteristics in several respects: The conversion of the endothermic reaction is determined by the temperature plateau in the catalytic part and can be maintained at a constant level throughout the complete endothermic semicycle. The heat capacities of the process gases during the production and the regeneration step can be adjusted properly in order to achieve optimal heat recovery.

The concept has been implemented in a laboratory-scale set-up. A sketch of the reactor is shown in Fig. 1.14 (left). Point-wise heat generation at well-defined positions along the fixed bed is accomplished with a special gas distributor which is located in the central reactor axis and has openings at four axial positions. The distributor is activated during the exothermic semicycle. Air is supplied to the reactor through the openings and burns part of the fuel contained in the main stream. The combustion reaction is almost instantaneous and represents approximately a point heat source. This configuration prevents direct contact of oxygen with the catalytic fixed bed and protects the catalyst against oxidation. Moreover, uncontrolled combustion of carbonaceous deposits and its detrimental consequences can be excluded. Nevertheless, catalyst decoking is ensured by mild, endothermic reactions, for example, gasification or hydrogenation. The right-hand part of Fig. 1.14 shows the temperature profiles at the end of consecutive endothermic and exothermic semicycles in periodic steady-state operation. The length of the production and regeneration cycle was set to 3 minutes. During the production cycle a mean methane conversion higher than 98 % could be attained. Despite insufficient insulation and a high wall-to-volume ratio of the laboratory set-up, a production capacity of 1.5 $kW_{LHV,H2}$ L^{-1} was achieved with a thermal efficiency of approximately 70 % – that is, the heat loss is in the order of 40 % of the heat uptake for the reforming reaction.

1.3.1.3 **Symmetric Mode with Side Stream Injection**

Side stream injection provides a flexible basis for new process variants. A derivate of this concept is the symmetric process: Shifting the combustion into an external combustion chamber and feeding the hot effluent gases to the main reactor enables a continuous heat supply to the endothermic reaction, and continuous production. The endothermic reaction mixture is fed in periodically changing directions to the reactor, and this leads to symmetric conditions during both semicycles. The advantage over the simultaneous mode is the exclusion of direct contact and of undesirable side reactions of the endothermic reaction mixture with oxygen. The symmetric process is particularly suitable for mole-number-increasing reactions since dilution of the reaction mixture with inert gases may shift the chemical equilibrium towards higher conversion. Accordingly, the symmetric process has been applied to styrene synthesis [23, 27]. Side feed can be added either through a single or multiple ports. Distributed side feeding provides additional control variables, such as periodic activation of the side ports [27]. This can be utilized for optimizing the shape of the temperature profile with respect to product selectivity. However, improved controllability and variability of the symmetric process goes along with a significantly increased complexity of the reactor design. Fine-structured inlet manifolds and static mixers are required in order to achieve a uniform distribution of the side feed over the reac-

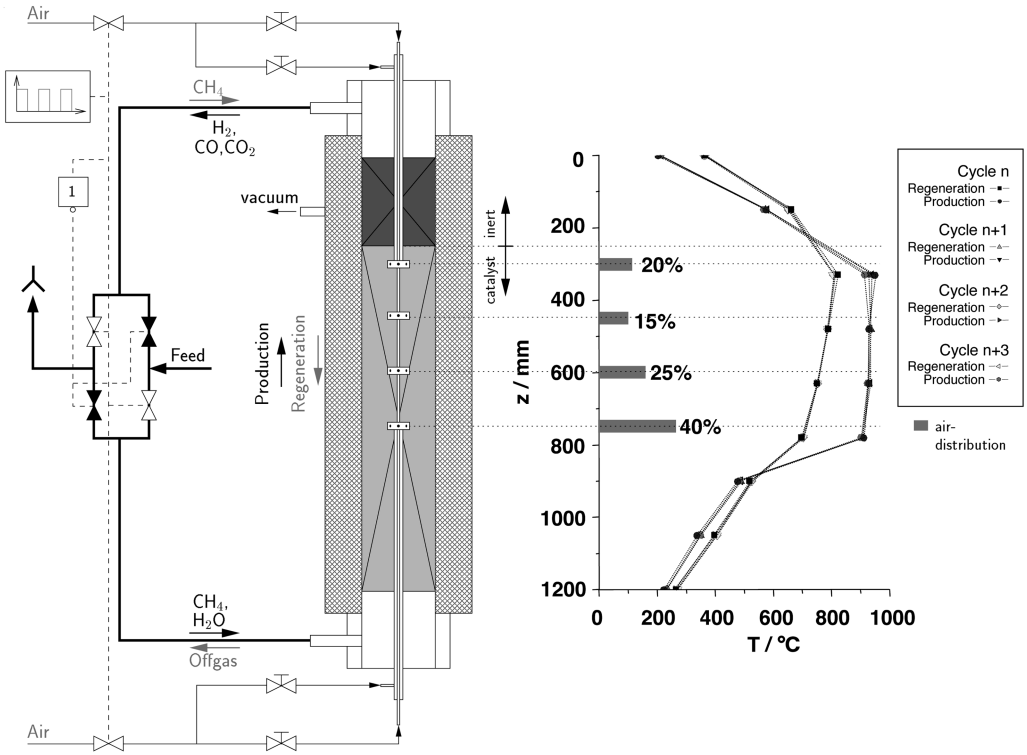

Fig. 1.14. Experimental proof-of-concept of asymmetric operation with distributed air feed [26]. Left: Schematic set-up of the bench-scale reformer. Right: Periodic steady-state temperature profiles at the beginning of successive cycles.

tor cross section. Besides, a significant temperature excess and a large side stream flow rate is required in order to introduce the process heat. A high side feed temperature may collide with the thermal stability of the reaction mixture, of the catalyst or the reactor material itself. A large side stream is detrimental for the thermal efficiency of heat recovery, due to the resulting inequality of upstream and downstream flow rates in the heat transfer sections (as discussed in Section 1.2.1.1). In the case of styrene synthesis heat losses due to incomplete heat recovery are typically 70–100 % of the heat consumption of the reaction.

1.3.1.4 **Counter-cocurrent Mode**

Van Sint Annaland [28] proposed a four-step process for propane dehydrogenation coupled with combustion of methane or propane; the phases of the process are illustrated in Fig. 1.15. Different process schemes are possible, depending on the sequence of the phases within one cycle. In any case, the complete cycle is symmetric, which is favorable with respect to heat recovery.

The most suitable variant comprises the following sequence of steps: combustion in forward flow direction–dehydrogenation forward–combustion backward–dehydrogenation backward. Model-based analysis reveals the importance of matching the kinetics of the endothermic and exothermic reactions in order to establish the desired temperature profile. Therefore, axial structuring of the fixed bed is crucial. An optimized reactor design (Fig. 1.16) comprises inert heat transfer sections at both ends of the reactor in order to avoid back-reaction. Adjacent to the end zones, sections of low catalytic activity are provided where the combustion mainly takes place, whilst the central section is filled with highly active dehydrogenation catalyst. Additionally, a mixture of propane and less reactive methane can be used as fuel, in order to adjust the temperature level in the central part of the reactor. The reaction zones of combustion and dehydrogenation are separated from each other. Considerably higher flow rates during the exothermic phases $\left(\dot{M}_{exo} : \dot{M}_{endo} = O(10)\right)$ Mare required for carrying the heat of combustion into the dehydrogenation zones. The conversion of the dehydrogenation reaction is uniform over the entire period of the production cycles. The heat loss due to incomplete heat recovery in the case shown is approximately 90 % of the generated heat, and is thus a multiple of the heat utilized by dehydrogenation.

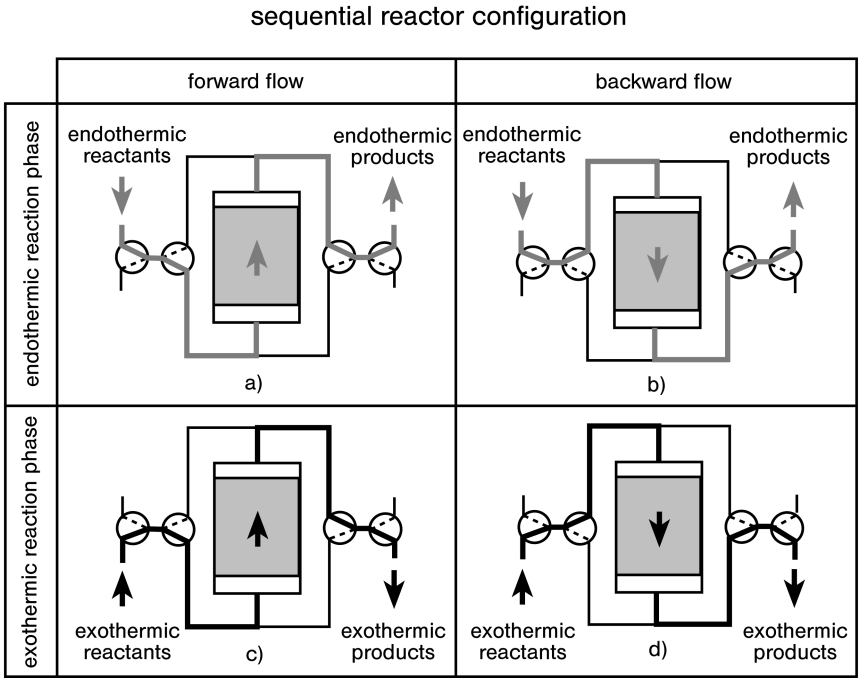

Fig. 1.15. Coupling of propane dehydrogenation and methane combustion in a four-step catalytic fixed-bed process [28].

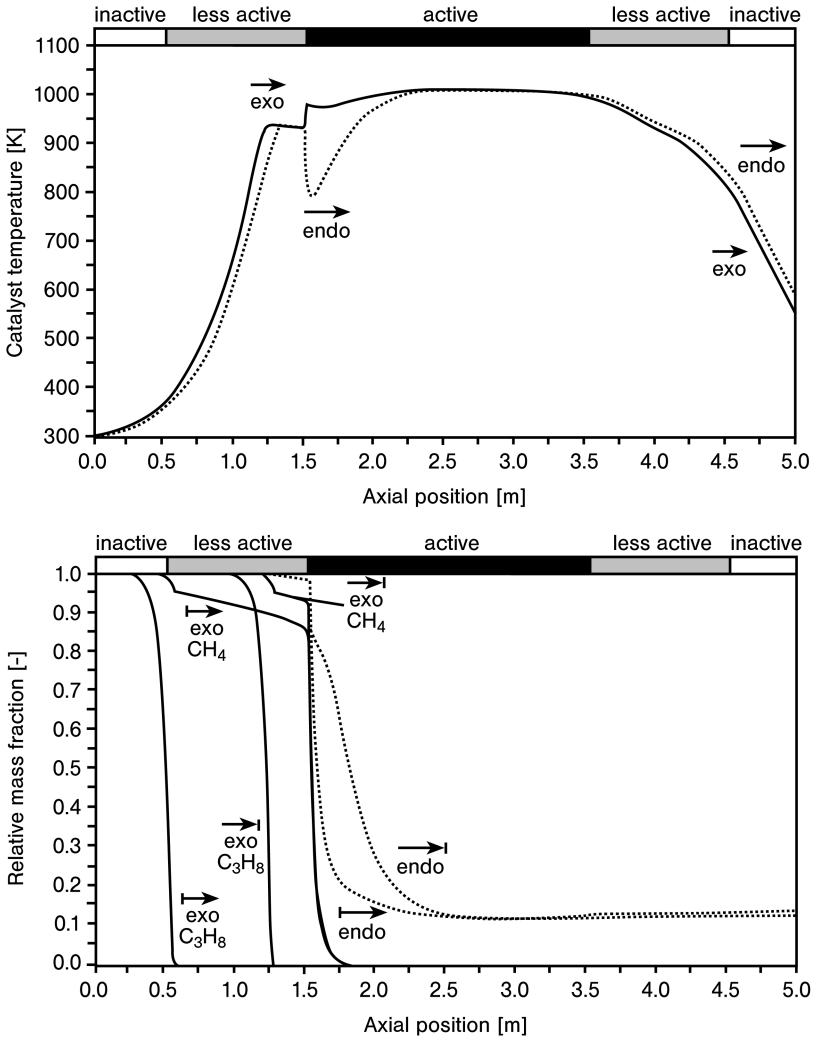

Fig. 1.16. Four-step propane dehydrogenation process [28]: Temperature profiles (top) and mass fraction profiles (bottom) at the end of the first two steps (1- exo, 2- endo). The end profiles of the subsequent steps are mirror images of the profiles shown.

This study also addresses the detrimental effect of carbonaceous deposits formed during the dehydrogenation steps. The ignition of accumulated coke during the subsequent regeneration step can lead to extreme local temperature peaks that are able to deactivate the catalyst or even to destroy the reactor. The phenomenon of temperature excursion during the exothermic gas–solid reactions has been analyzed by Nieken and Watzenberger [29] and Salden [30], and will be discussed briefly in the following section.

1.3.1.5 Overheating During Oxidative Coke Removal

Regenerative processes for hydrocarbon processing include oxidative coke removal as an integral part of the process cycle in order to sustain a high catalytic activity. However, the results of both experimental and theoretical studies agree that oxidative coke removal may lead to severe, uncontrollable temperature excursions [13, 14, 28]. This phenomenon is elucidated in the following text in order to identify the reasons for this critical behavior, as well as to suggest possible remedies, based upon an analysis given in Ref. [30].

We assume a fixed-bed of semi-infinite axial extension with a uniform initial temperature T_{fb}^2 and coke loading q_B^0. We further neglect dispersive effects and assume that coke combustion is an instantaneous reaction. Passing a gas stream with inlet temperature T^+ and inlet oxygen concentration c_{O2}^+ at a flow rate v^0 through the fixed-bed, typically two stationary traveling fronts are formed (Fig. 1.17). The propagation velocity of the thermal front w_{therm} depends on the heat capacity of the gas and the fixed bed (Eq. (7)). The propagation velocity of the reaction front is given by the following expression

$$w_R = \frac{c_{O2}^0}{q_B^0} v^0 \tag{9}$$

resulting from the stoichiometry of complete coke combustion:

$$C + O_2 \rightarrow CO_2$$

Hence, w_{therm} and w_R are independent of each other. The effective temperature rise depends on the ratio of w_{therm} and w_R and can be estimated based on the following simplified considerations.

In a quasi-homogeneous model, the evolution of the temperature T_{fb}, the coke loading q_B, and the oxygen concentration c_{O2} are given by the following set of equations:

$$(\rho c)\frac{\partial T_{fb}}{\partial t} = -\left(\rho c_p\right)_g v \frac{\partial T_{fb}}{\partial z} + \left(-\Delta H_R\right) r \quad T_{fb}(z=0,t) = T^+;\ T_{fb}(z,t=0) = T_{fb}^0 \tag{10}$$

$$\frac{\partial q_B}{\partial t} = -r \qquad q_B(z,t=0) = q_B^0 \tag{11}$$

$$0 = -v^0 \frac{\partial c_{O2}}{\partial z} - r \qquad c_{O2}(z=0,t) = c_{O2}^+ \tag{12}$$

Transformation of the above system into moving coordinates $\tau = t$; $\zeta = z - w_{therm}\, t$ yields:

$$(\rho c)\frac{\partial T_{fb}}{\partial \tau} = (-\Delta H_R) r \qquad T_{fb}(\zeta, \tau = 0) = T_{fb}^0 \tag{13}$$

$$\frac{\partial q_B}{\partial \tau} = w_{therm}\frac{\partial q_B}{\partial \zeta} - r \quad q_B(\zeta,\tau=0) = q_B^0 \; ; \quad q_B(\zeta\to\infty,\tau) = q_B^\infty \tag{14}$$

$$0 = -\nu^0 \frac{\partial c_{O2}}{\partial \zeta} - r \qquad c_{O2}(\zeta=0,\tau) = c_{O2}^+ \tag{15}$$

Additionally, the constant pattern assumption implies the following conditions:

$$\frac{\partial T_{fb}}{\partial \tau} = -\left(w_R - w_{therm}\right)\frac{\partial T_{fb}}{\partial \zeta} \tag{16}$$

$$\frac{\partial q_B}{\partial \tau} = -\left(w_R - w_{therm}\right)\frac{\partial q_B}{\partial \zeta} \tag{17}$$

Eq. (17) inserted in Eq. (14) yields:

$$-\left(w_R - w_{therm}\right)\frac{\partial q_B}{\partial \zeta} = w_{therm}\frac{\partial q_B}{\partial \zeta} - r \tag{18}$$

$$\Rightarrow r = w_R\frac{\partial q_B}{\partial \zeta} \tag{19}$$

Combining Eqs. (13), (16), and (19) leads to:

$$-\left(\rho c\right)\left(w_R - w_{therm}\right)\frac{\partial T_{fb}}{\partial \zeta} = \left(-\Delta H_R\right)\; w_R\frac{\partial q_B}{\partial \zeta} \tag{20}$$

$$\Rightarrow \frac{dT_{fb}}{dq_B} = -\frac{w_R}{w_R - w_{therm}}\cdot\frac{\left(-\Delta H_R\right)}{\left(\rho c\right)} \tag{21}$$

Here, we must discriminate between two cases:

1. Reaction front faster than thermal front ($w_R > w_{therm}$):

$$\Delta T = T_{fb}^0 - T_{\max} = -\frac{w_R}{w_R - w_{therm}}\cdot\frac{\left(-\Delta H_R\right)}{\left(\rho c\right)}\cdot q_B^0 = -\frac{w_{therm}}{w_R - w_{therm}}\cdot\frac{\left(-\Delta H_R\right)}{\left(\rho c_P\right)_g}\cdot c_{O2}^+ \tag{22}$$

$$\Rightarrow \Delta T_{eff} = \frac{1}{\frac{\left(\rho c\right)}{q_B^0} - \frac{\left(\rho c_P\right)_g}{c_{O2}^+}}\cdot\left(-\Delta H_R\right) \tag{23}$$

This case, displayed in Fig. 1.17(c), occurs at high inlet oxygen concentrations or small initial coke loading – that is, the combustion is limited by the amount of coke. The heat generation by reaction exceeds the heat consumption for heating

up the cold gas stream. For $w_R >> w_{therm}$ the effective temperature rise approaches asymptotically the value

$$\Delta T_{ad}^{s} = \frac{q_B^0(-\Delta H_R)}{\rho c}$$

that can be interpreted as the adiabatic temperature rise of the solid phase.

2. Reaction front slower than thermal front ($w_R < w_{therm}$):

$$\Delta T = T^+ - T_{\max} = \frac{w_R}{w_R - w_{therm}} \cdot \frac{(-\Delta H_R)}{(\rho c)} \cdot q_B^0 = \frac{w_{therm}}{w_R - w_{therm}} \cdot \frac{(-\Delta H_R)}{(\rho c_P)_g} \cdot c_{O2}^+ \tag{24}$$

$$\Rightarrow \Delta T_{eff} = \frac{1}{\frac{(\rho c_P)_g}{c_{O2}^+} - \frac{(\rho c)}{q_B^0}} \cdot (-\Delta H_R) \tag{25}$$

This case, displayed in Fig. 1.17(d), occurs at a low inlet oxygen concentration or a high initial coke loading – that is, the combustion is oxygen-limited. The heat of combustion is carried away downstream by convection. For $w_R << w_{therm}$ the effective temperature rise approaches asymptotically the value

$$\Delta T_{ad}^{g} = \frac{c_{O2}^+(-\Delta H_R)}{(\rho c_p)_g}$$

which can be interpreted as the adiabatic temperature rise of the gas phase.

Figure 1.18 displays the effective temperature rise during oxidative coke removal as a function of the oxygen molar fraction of the regeneration gas according to Eqs. (23) and (25), respectively. The adiabatic temperature rise of the shown case is 38 K. However, ΔT_{eff} can be much higher and tends to infinity at the limit of $w_R \to w_{therm}$. This can be explained as follows: when the velocities of the thermal front and the reaction front are equal, the heat of combustion accumulates in a narrow zone which may lead to extremely high local temperatures. This conclusion has been verified theoretically through detailed simulations [30].

The above considerations hold under the condition that the ignition temperature of coke combustion is lower than T_{fb}^0 in the coke-limited regime, or lower than T^+ in the oxygen-limited regime. However, in the considered heat-integrated processes the feed temperature T^+ is generally far below the ignition temperature. The fatal aspect in this scenario is that coke regeneration is carried out "carefully" – that is, with a low oxygen concentration. Oxygen deficiency leads to incomplete coke removal according to the following condition:

$$w_R = w_{therm} = \frac{c_{O2}^+}{q_B^0 - q_B^r} \cdot \nu^0 \tag{26}$$

In this way, the reaction front is synchronized inevitably with the thermal front, leading to the observed temperature excursions (Fig. 1.19).

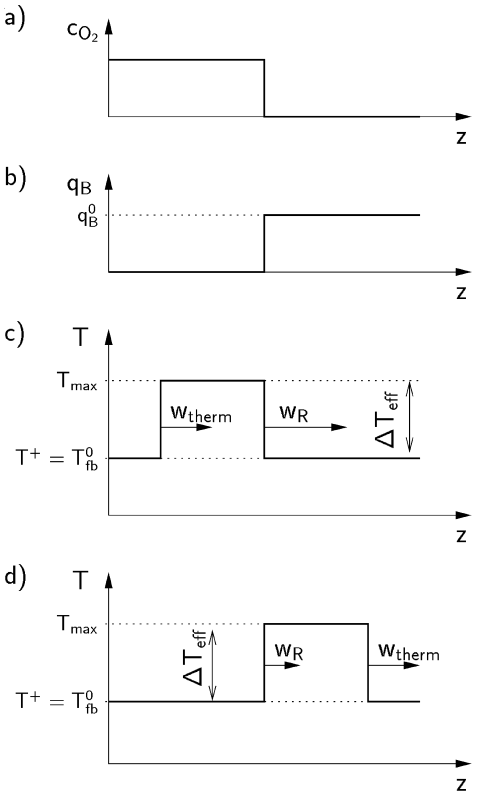

Fig. 1.17. Schematic picture of front propagation during oxidative coke removal. (a) Oxygen concentration in the regeneration gas, e.g., air. (b) Coke loading of the solid phase. (c) Front propagation of the thermal front (velocity w_{therm}) and the reaction front (w_R) with preceding reaction front. (d) Front propagation with preceding thermal front (special case: $T^+ = T_{fb}^0$).

Hence, in order to prevent overheating it is not simply the amount of coke that matters; rather, it is also necessary to avoid synchronization of the thermal and combustion fronts. This can be achieved by correctly adjusting the oxygen inlet concentration, in order to carry out regeneration in the coke-limited regime.

1.3.2 Recuperative Processes

The activities of heat-integrated processes with recuperative heat exchange are mainly devoted to the conversion of primary fuels (hydrocarbons or alcohols) to hydrogen, with few exceptions – for example, investigations on the dehydrogenation of light alkanes in Schmidt's group [3]. The practical relevance and vitality of

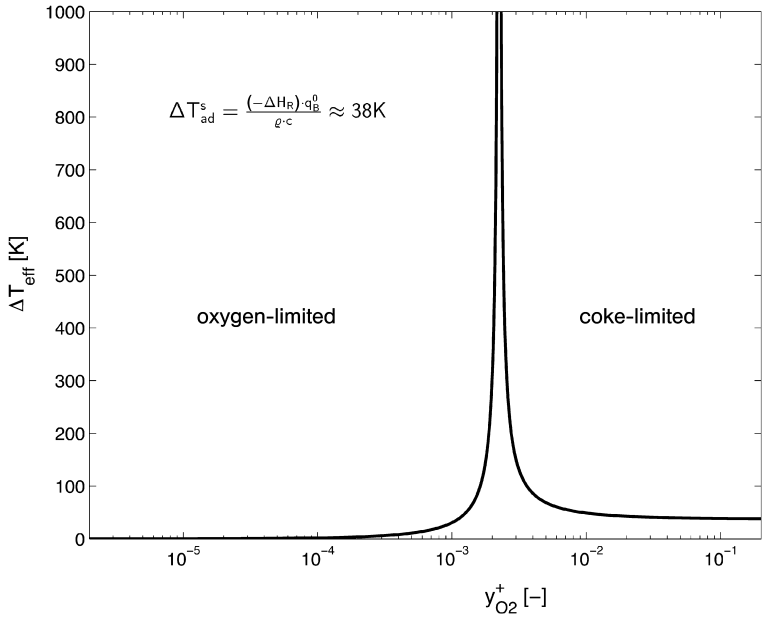

Fig. 1.18. Effective temperature rise during oxidative coke removal as a function of the oxygen mole fraction of the regeneration feed gas.

research on heat-integrated fuel processors can be estimated from the number of established companies and start-ups active in this area [31]. Two major trends prevail: One focusing on optimization of existing concepts and one aiming at novel concepts based on micro-reactors.

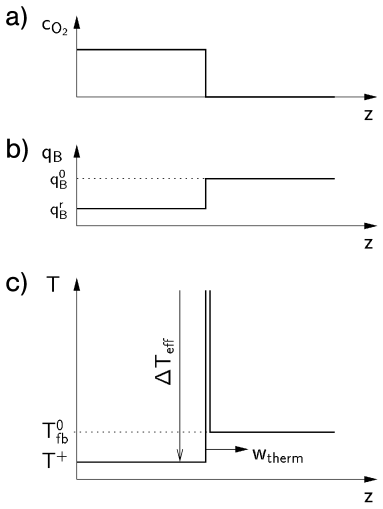

Fig. 1.19. Front propagation during oxidative coke removal with low inlet temperature. (a) Oxygen concentration in the regeneration gas. (b) Coke loading of the solid phase. (c) Development of temperature excursion in the propagating reaction zone.

1.3.2.1 Processes for Large-Scale Applications

Processes developed on the basis of conventional reforming technology are designed for large-scale hydrogen production, for example in chemical plants, power plants or hydrogen filling stations. Optimized designs aim at reduction of waste heat generation at a level that renders steam export obsolete.

ICI developed a two-stage process comprising a gas-heated tubular fixed-bed reformer (GHR) interconnected with an autothermal reformer for industrial syngas generation [32, 33]. The term autothermal reforming (ATR) is used for the simultaneous coupling of reforming and oxidation. Figure 1.20 shows a scheme of this combined process. About 25 % of the hydrocarbon is converted in the GHR, with the product stream being redirected into a concentric tube before leaving the GHR. The gas is cooled down through countercurrent heat exchange with fresh gas, before entering the ATR stage where conversion is completed. The hot syngas from the ATR passes through the GHR supplying additional heat to the steam-reforming process.

The Haldor Topsøe Convection Reformer (HTCR) has been developed for the production of hydrogen from hydrocarbons without steam generation. The elementary unit of the reformer consists of two concentric tubes (Fig. 1.21). The annular space

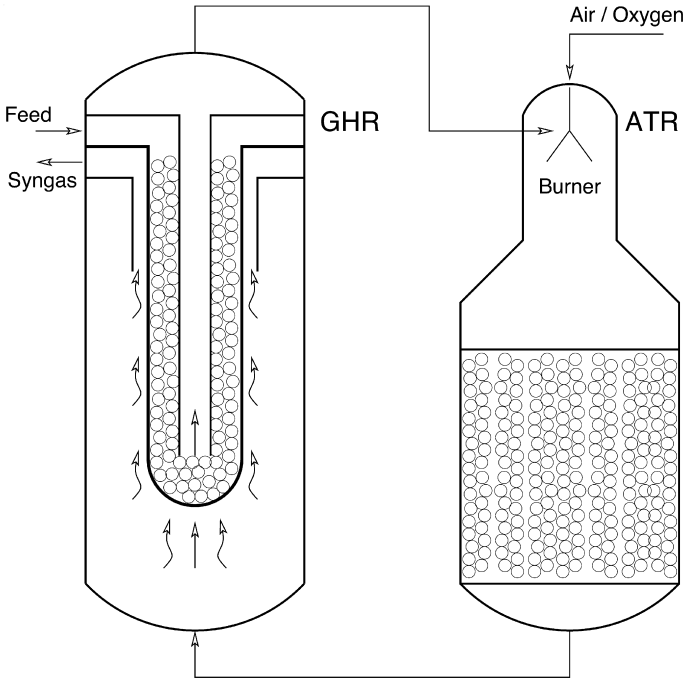

Fig. 1.20. Autothermal syngas generation by combining simultaneous autothermal reforming in an air/oxygen-fired fixed-bed reactor (ATR) and steam reforming in a gas-heated tubular fixed-bed reactor (GHR) [32, 33].

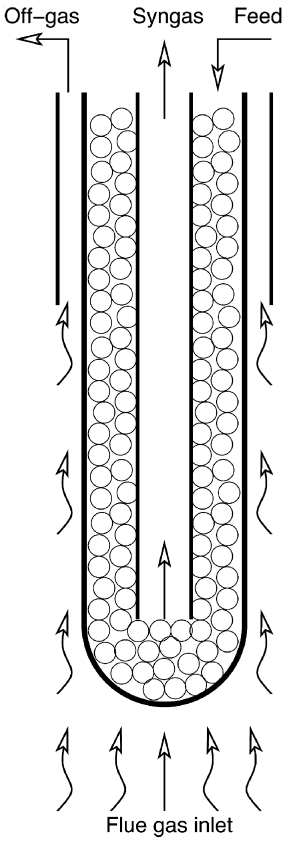

Fig. 1.21. Schematic set-up of the heat-integrated HTCR process for industrial syngas production by steam reforming of natural gas.

between the two tubes is filled with catalyst. Feed gas enters the outer tube at one end, while the other end is closed. In this way, countercurrent heat exchange is attained between the product stream in the inner tube and fresh gas in the annular space. A bundle of these modules is inserted into a furnace, where the combustion of fresh gas and off-gas from the hydrogen purification unit produces the process heat. The hot flue gas is conducted upwards and supplies heat to the reforming process, for overheating of the reaction mixture and for steam generation. In this way, the HTCR process enables almost complete recovery of the sensible heat of the process gases. According to technical data presented by the manufacturer, the HTCR process has an overall thermal efficiency of $\eta = LHV_{H_2^{prod}}/LHV_{CH_4^+} = 72\%$ with zero steam export.

A concept with a higher degree of heat integration is described in Ref. [34]. The concept has been derived from the FLOX burner (FLOX = flameless oxidation in the gas phase) [35]. This combustion regime can be attained with highly preheated fresh air in combination with intensive recirculation in the combustion chamber, and features extremely low emissions. Fresh air preheating is accomplished in the FLOX burner through countercurrent heat exchange with the hot flue gases in an

integrated heat exchanger. Thus, heat recovery is inherently included in the FLOX burner. In the FLOX reformer the reforming modules consisting of two concentric tubes, similar to those of the HTCR- and ICI-GHR design, which hang in the combustion chamber. Steam generation, reforming and water-gas-shift reaction are integrated in every module. Figure 1.22 shows a scheme of the heat management of this concept. The two heat recovery loops of the reforming and combustion gas are almost completely separated from each other. The heat content of the reforming gas is utilized for vaporizing the liquid water and the water-gas shift stage for CO-removal is cooled by the produced steam. The sensible heat of the flue gas is utilized for preheating the fresh air superheating the methane/steam mixture. The FLOX-reformer design is modular with a capacity of 50–250 $Nm^3\ H_2\ h^{-1}$. Thermal efficiency exceeds 80 %.

1.3.2.2 **Processes for Small-scale Applications**

Nowadays, the most common small-scale application of hydrogen is the use in residential or mobile fuel cell systems. Special requirements of this application are compact design, integrated CO-removal, high energetic efficiency, quick start-up and fast transient behavior. The proposed solutions comprise unit-operation-based concepts as well as multifunctional, micro-structured reactors.

A gasoline processing system has been developed by Daimler Chrysler [36] based on ATR. Catalytic ATR is extremely rapid, and provides the potential for a very compact process. The specific productivity of the ATR is about 15 $kW_{LHV,gasoline}\ L^{-1}$. The fuel is sprayed into a preheated air stream. The ATR-product stream enters a high-temperature shift reactor (HTS), in order to convert CO. Both ATR and HTS are designed as adiabatic metallic monolith reactors, which are coated with different noble metal catalysts for reforming and water-gas shift reactions. The operation temperature of the ATR is above 750 °C, while the HTS operates at about 450 °C. Therefore, it is recommended that the two units are interconnected with a heat exchanger, in order to recover the heat of the ATR product stream for preheating the ATR feed (Fig. 1.23). The behavior of the coupled system has been analyzed in Ref. [37].

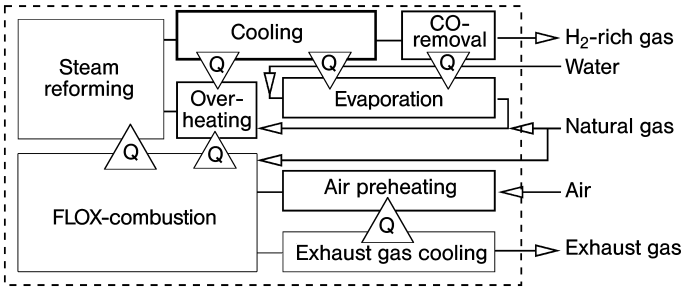

Fig. 1.22. Flowsheet of the FLOX-reformer. The triangles indicate the exchanged heat fluxes between different stages of the process [34].

One major conclusion of this study is that integrated heat recovery reduces the sensitivity of the process against fluctuations of the operating parameters, and thus enhances the feasible operation range. The effect of heat recovery during a load change is illustrated in Fig. 1.24. The stationary temperature profiles are shown at gasoline loads equivalent to 3 and 33 kW_{LHV} of gasoline. The temperature profile at the inlet of the ATR is dominated by the fast oxidation, while steam reforming of gasoline takes off further downstream. At high load, the temperature maximum could exceed the allowed limit. In contrast, if heat generation falls below a certain threshold, the heat losses become dominant and the reactor extinguishes. Heat recovery stabilizes the operating conditions in the following way: At high load the efficiency of heat recovery declines and the inlet to the ATR stage drops. This compensates partially the temperature rise in the combustion zone of ATR and limits the peak temperature. At low load the efficiency of heat recovery improves, and hence the inlet temperature of the ATR increases. This stabilizes the ignited state. Experimental studies confirm that integrated heat recovery enables a loading variation of 1:10 and contributes to a fast and smooth transient behavior.

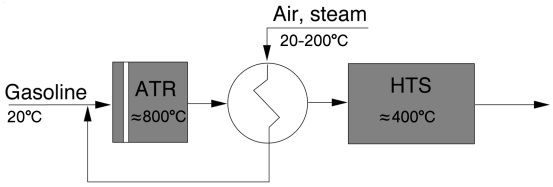

Fig. 1.23. Flowsheet for a heat-integrated system of an autothermal gasoline reformer (ATR) and a high-temperature shift stage (HTS) interconnected with a heat exchanger [37].

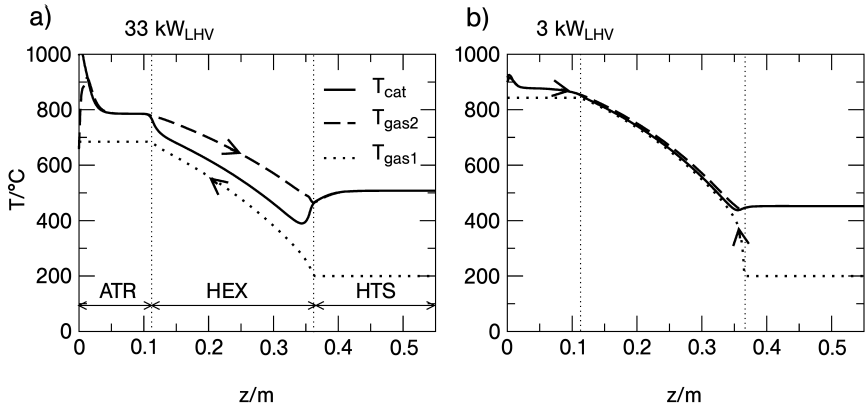

Fig. 1.24. Steady-state, axial temperature profiles for the gasoline reformer in Figure 1.21. (a) High load: 33 kW_{LHV}; (b) low load: 3 kW_{LHV}.

The progress in micro-reactor technology provides the background for the development of compact fuel processors and peripheral components of fuel cell systems.

Published performance data [38–42] indicate the high development status already reached: Volume-specific productivity values up to 750 $l_N H_2/lit./h \equiv 2{,}3\ kW_{LHV,H2}/lit.$ and overall thermal efficiency values from 80 to 90 % have been reported for gas generation processes including feed preheating, gas generation and purification. Unfortunately, no further details are available about reactor design and the process conditions except for very few of them.

The Integrated Fuel Processor (IFP)

This was developed by Ballard Power [40], and is a multifunctional reactor including the evaporation of a methanol/water mixture, autothermal methanol reforming and preferential oxidation (PrOx) for CO removal. The device consists of a stack of identical, structured plates which divide its volume in two compartments with microstructured rectangular channels. These plates are made from aluminum and copper, thus ensuring high thermal conductivity for a uniform temperature over the entire reactor volume. A schematic picture of a single plate is shown in Fig. 1.25. Liquid methanol/water mixture enters the first compartment and evaporates when heated by the exothermic PrOx reaction, which takes place on the other side of the plate. The reactants are mixed with air and enter the porous section of the plates where the reforming reaction takes place as the reaction gases cross the plates. In the second chamber, secondary air is added and the reaction products pass over a PrOx-catalyst while exchanging heat with the first chamber. The temperature of the reactor is adjusted to 280 °C. Proof-of-concept experiments with the IFP gave an extremely high productivity of 2.5 $m_N^3\ H_2/lit./h \equiv 7.5 kW_{LHV,H_2}/lit.$ A special powder-metallurgical fabrication method allows for producing impermeable and porous areas on the plate as required for the flow distribution, embossing the surface structure and impregnating with reforming catalyst (Cu/ZnO) in one step. The plates are piled to a stack and joined by sintering. However, the IFP-design is not suitable for high-temperature applications such as gasoline or methane processors. Furthermore, the above-mentioned autothermal reforming processes are charged with the inherent shortcomings of the simultaneous mode with regard to product dilution and pressure limitations. Therefore, the focus is set on high- temperature steam reforming. The potential of catalytic plate reactors with narrow channels regarding controllability, productivity and efficiency has been demonstrated in detailed theoretical studies by Zanfir and Gavriilidis [43]. One crucial task in implementing the concept is the development of fabrication techniques for catalytic activation of the plates and for assembling a stack. The solution of choice would be to coat the plates before joining them to a stack. However, the conditions required by the common joint methods – soldering or diffusion bonding – would damage the catalyst, whilst the alternative of laser welding is too expensive. Therefore, although coating the completely assembled reactor is often employed as the only viable solution, this is extremely difficult to control [44] and is a clear restriction of the adequacy of micro-fabricated reactors for specific applications. Moreover, the suggestion of "the smaller the better" is not

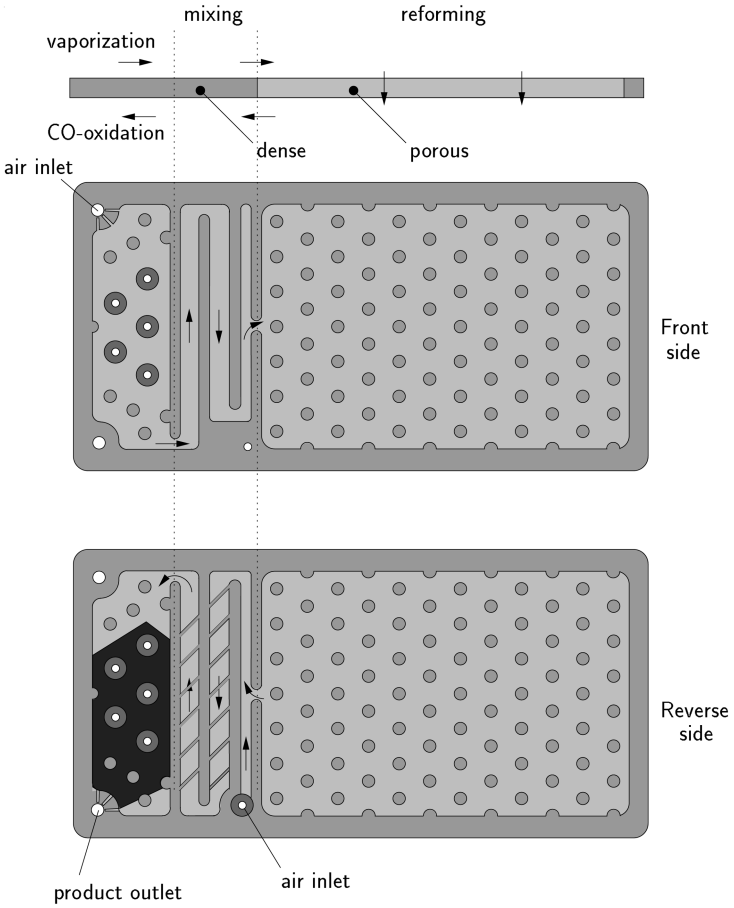

Fig. 1.25. Schematic diagram of a single plate of the Integrated Fuel Processor (IFP) [40]. Top = flow scheme; center = view to the front side; bottom = view to the reverse side.

generally true in the context of processes with integrated heat recovery. Decreasing the channel width allows a given heat transfer area to be installed in shorter devices. This enhances the influence of heat conductivity and tends to equalize temperature gradients; thus, it is an advantage for temperature control in the reaction stage. However, the same effect considerably affects the efficiency of heat recovery in the heat exchanger sections [45]. Therefore, it is not recommended that attention be focused exclusively on minimization of the hydraulic diameter and the size of the devices.

Another important aspect is optimization of the process parameters. The challenge here is to control catalytic combustion, in order to attain overlapping of the combustion and reforming reaction over a sufficient interval [46]. The operating conditions are mainly determined by the fuel composition and the heat exchange

mode between the process streams. In low-temperature processes (e.g., methanol reforming) or in processes without feed preheating, hydrogen is required to stabilize the ignited state of the catalytic combustion [47, 48]. However, the presence of hydrogen is extremely critical at high temperatures due to the ignition of homogeneous combustion. The use of less-reactive pure methane is recommended in this case, in order to avoid runaway [49]. Additionally, countercurrent flow of the reforming and the combustion gas gives rise to separation of the reaction zones and to runaway of the combustion reaction. A considerable excess of the combustion gas flow rate against the reforming gas flow rate is required in order to stabilize reasonable operating conditions at the cost of a lower thermal efficiency [45]. Overlapping of the reaction zones could be enforced either through distributed side-feeding of air or fuel or through cocurrent flow of combustion and reforming gas stream in the catalytic part of the reactor [50].

A comprehensive concept including process and apparatus design has been developed based on the folded plate reactor design [51]. Comparable concepts are known from the Boreskov Institute of Catalysis [52]. The body of the reactor consists of a folded sheet of metal that divides its volume in two chambers, forming channels with rectangular cross-sections (Fig. 1.26). By applying this technique, the channel width can be adjusted individually at each side, depending on the respective heat of reaction and reaction kinetics: narrow channels (as small as 1 mm) are indicated for fast reactions, whereas wide channels (up to 10 mm) allow for the installation of sufficient amounts of catalyst for slow reactions. An important feature of the folded-sheet design is that all channels are accessible from the side over the entire reactor length. In this way, it is possible to distribute the feed at arbitrary positions, in order to specifically control the operating conditions. The frontal ends can be sealed (e.g., with silicon rubber) if they are permanently exposed to low temperatures; otherwise, welding or high-temperature soldering is used which ensures thermal stability up to 900 °C. In this way, the two chambers can be separated from each other with a minimum number of joints, and this reduces potential failure sources. The channels are filled with structured spacers; these play an important role in the reactor concept as they support the reactor walls, provide the mechanical stability to the

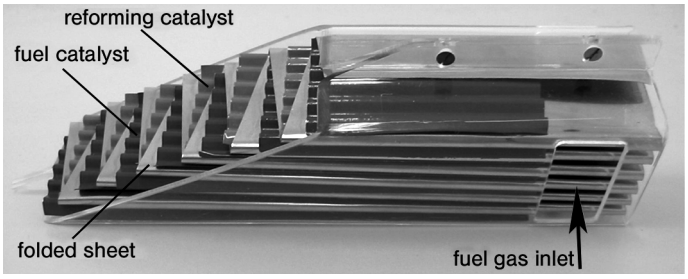

Fig. 1.26. Model of the folded sheet reactor with corrugated, catalyst-coated spacers.

reactor structure, and contribute to the improvement of the heat exchange through planar contact to the reactor wall. Spacers with crossing passages can be used as static mixers downstream of the injection ports in order to distribute the feed uniformly over the depth of each channel; finally, the spacers can be coated with catalyst. In this way, it is possible to adjust the axial structure of the channels in order to attain optimal implementation of multiple functions. The gas inlet and outlet ports are integrated in shells, forming the reactor casing. They are assembled together by two longitudinal weld seams, and the casing can also be reinforced to enhance the rigidity of the device. Two prototype reactors have been developed – one for low-temperature methanol steam reforming, and one for high-temperature methane steam reforming based on the folded-sheet reactor concept.

Methanol steam reforming

The concept has been developed to the stage of a bench-scale prototype for $3m_N^3/h$ hydrogen [53]. The complete hydrogen generation process including evaporation of methanol and water, superheating, reforming, water-gas shift combined with product cooling, are integrated in this device. Heat supply is controlled by distributed side-feeding of fuel (hydrogen) at five stages along the reactor. The experiments showed a good methanol conversion ($X > 90\,\%$) with moderate CO formation ($\gamma_{co} \sim 2\,\%$) and excellent dynamics upon load changes.

However, the distribution of the fuel in the depth of the channels required a complex capillary distributor with tiny exit nozzles. The particular device, although optimal with regard to the uniformity of gas distribution, seems not to be an adequate technical solution.

Methane steam reforming

The counter-cocurrent reformer concept including two countercurrent heat exchangers and a cocurrent reaction section (Fig. 1.27(a)) was considered in order to attain optimal conditions for kinetic control of the combustion [8]. It is well known that cocurrent cooling is generally favorable in preventing runaway of highly exothermic reactions. In the particular case, chemical cooling is provided by the reforming reaction.

The conditions in the reaction section are of primary interest for the entire process. Experiments have been conducted with superheated feed streams using a three-channel model reactor in order to analyze the coupling of methane reforming and methane combustion in the cocurrent mode. Figure 1.27(c) shows a sketch of the configuration representing an elementary unit of the folded sheet reactor with a combustion channel of full-height in the middle and two reforming channels of half of full- height, one on each side. Heat losses to the surroundings have been partially compensated by an electrically heated insulation. The diagrams show the temperature profile (Fig. 1.27(b)) and the performance data of the reactor (Fig. 1.27(d)) depending on the fuel concentration in the steady state. The most important result is that the cooling effect of the reforming reaction effectively prevents runaway of combustion. Hence, it is possible to achieve complete conversion under moderate

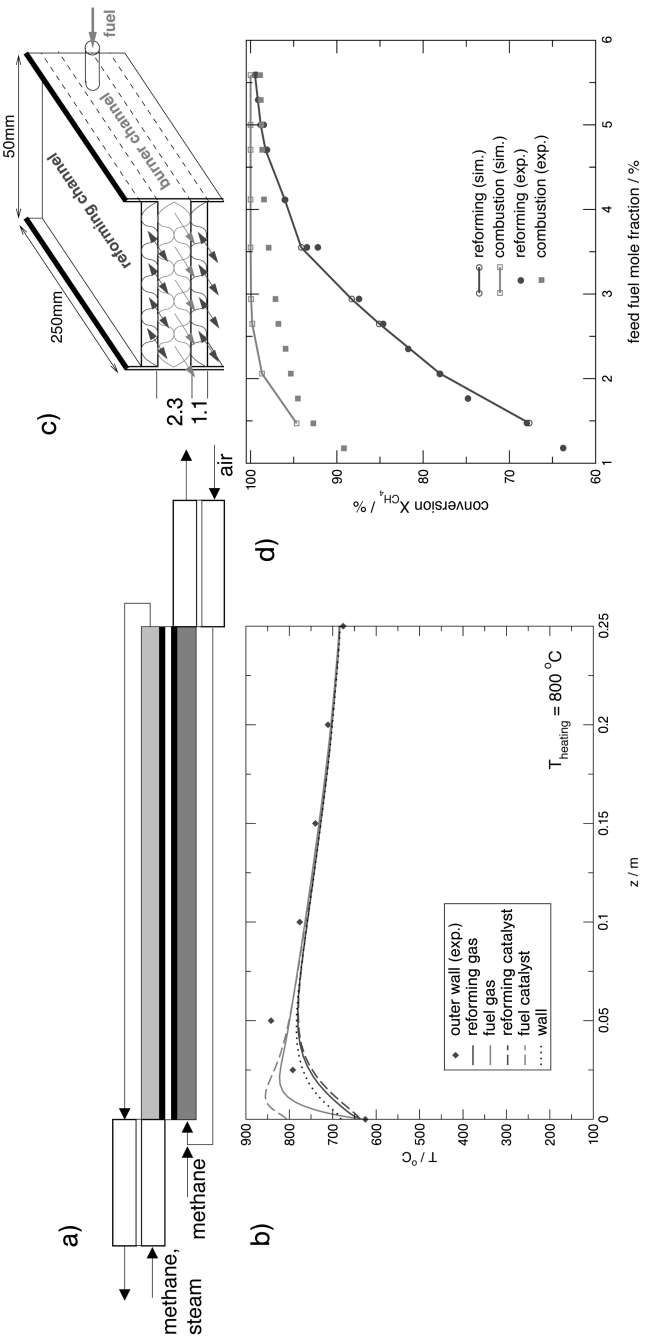

Fig. 1.27. Methane steam reformer with cocurrent flow in the reaction zone. (a) Flow scheme. (b) Simulated and measured temperature profiles in the reaction zone of the three-channel reactor. (c) Sketch of the three-channel reactor for coupling of steam reforming and combustion. (d) Simulated and measured methane conversion depending on fuel feed concentration of the combustion reaction.

conditions. Furthermore, the generated excess heat can be varied through proper adjustment of the amount of fuel added. This defines the temperature difference between the exit and inlet which is the driving force for heat recovery in the subsequent heat exchange sections. Experiments conducted with the three-channel reactor proved that the efficiency of thermal coupling of combustion and reforming could be increased far beyond the common values of the state-of-the-art processes. Indeed, up to 85 % of the generated heat can be utilized by the reforming reaction despite the heat losses of the experimental set-up. Figure 1.28 shows schematically the general reactor design, along with simulated temperature and conversion profiles. The additional side stream feeding port enables to control the temperature in the reforming stage at varying loads. According to the simulation results, 90 % of the released heat of combustion is expected to be taken up by the reforming reaction. The specific production capacity is estimated as 2.5 $m_N^3\, H_2/h/Liter_{reactor}$.

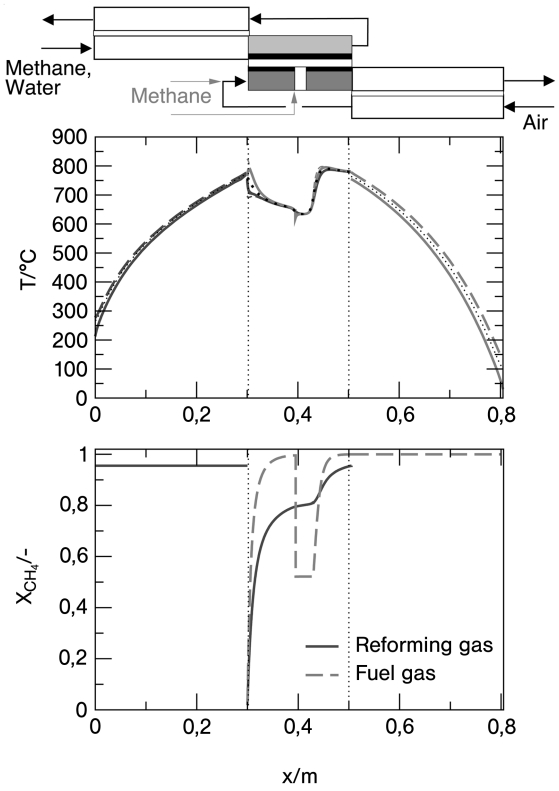

Fig. 1.28. Integrated, autothermal methane reformer with cocurrent flow in the reaction zone and countercurrent heat recovery. Simulated steady-state temperature and conversion profiles.

Experimental proof-of-concept with a bench-scale reactor (production capacity of 3.3 m_N^3 H_2/h) is the subject of ongoing investigations.

1.4 Conclusions

The coupling of high-temperature endothermic and exothermic reactions in multifunctional devices with integrated heat recovery is gaining increasing interest, driven in particular by the developing hydrogen technology. Conventional concepts are not suitable to meet the demands on specific performance, thermal efficiency and autonomy of the process. Two routes are currently being pursued towards novel solutions employing either regenerative or recuperative heat exchange for heat coupling and heat recovery.

Regenerative processes based on the reverse-flow reactor concept are preferred in large-scale applications due to their simple and scalable reactor design. Compact recuperative concepts based on the wall reactor concept provide the best potential for small-scale applications. Apart from these general features, correct structuring of the catalytic and fluid-dynamic properties of the reactor is essential for an optimal design. Distributed feeding of combustion air or fuel ensures optimal heat transfer from the exothermic to the endothermic part. An integrated approach combining apparatus design and process development is indicated for optimal implementation of novel solutions.

With regard to fuel processors for hydrogen production, autothermal reforming processes have initially approached the technological and economical targets for technical implementation, though their applicability is limited due to principal shortcomings of the concept. Properly designed steam reforming processes may possibly compete with autothermal reformers with regard to space–time yield and heat recovery, while offering high flexibility in terms of operating conditions. They may, therefore, be utilized in a wide spectrum of applications.

Symbols and Abbreviations

A	area, m^2
c	specific heat capacity of the solid phase, J kg^{-1} K^{-1}
c_p	specific heat capacity of the gas phase, J kg^{-1} K^{-1}
c_j	concentration of component j, mol m^{-3}
D_i	inner diameter, m
h	heat capacity ratio
h	specific enthalpy, J mol^{-1}
k_h	heat transfer coefficient, W m^{-2} K^{-1}
$loss_{norm}$	normalized heat losses
$\dot{M}$	mass flux, kg s^{-1}
$\dot{N}$	molar flux, mol s^{-1}
NTU	number of transfer units

p	pressure, bar
q_B	coke loading, mol m^{-3}
r	reaction rate, mol m^{-3} s^{-1}
t	time, s
T	temperature, K
v^0	superficial gas velocity, m s^{-1}
w_{therm}	thermal front propagation velocity, m s^{-1}
$w_{endo/exo/R}$	reaction front propagation velocity, m s^{-1}
X	conversion of reaction
y_j	molar fraction of the component j
z	axial coordinate, m

Greek letters

α_w	heat transfer coefficient, W m^{-2} K^{-1}
ΔH_R	heat of reaction, kJ mol^{-1}
ΔT	temperature difference, K
ΔT_{ad}	adiabatic temperature rise, K
ΔT_{eff}	effective temperature rise, K
λ	axial heat conductivity, W m^{-1} K^{-1}
ρ	density, kg m^{-3}
τ	time in transformed system of coordinates, s
ζ	spatial coordinate in transformed system, m

Indices

0, +	inlet or initial conditions
–	outlet conditions
c	fixed-bed catalyst
cyc	cycle
equ	equilibrium conditions
endo	endothermic reaction
exo	exothermic reaction
fb	fixed-bed
g	gas phase
l	liquid phase
lat	latent heat storage
low	lower value
max	maximum value
prod	production cycle
reg	regeneration cycle
ref	steam reforming
s	solid phase
w	separating wall

Acronyms

ATR	Autothermal Reformer
GHR	Gas-Heated Reformer
HTS	High-Temperature Shift Stage
LHV	Lower Heating Value
PrOx	Preferential Oxidation

References

1. Horizon 2015: *Perspectives for the European Chemical Industry. A study by the European Chemical Industry Council* (www.cefig.org), 2004.
2. J. Larminie, A. Dicks, *Fuel Cell Systems Explained*. 2nd edn., Wiley, 2003.
3. K. Venkataraman, J. M. Redenius, L. D. Schmidt, Millisecond Catalytic Wall Reactors: Dehydrogenation of Ethane. *Chem. Eng. Sci.,* **2002**, *57,* 2335–2343.
4. K. Venkataraman, E. C. Wanat, L. D. Schmidt, Steam Reforming of Methane and Water Gas Shift in Short Contact Time Reactors. *AIChE J.,* **2003**, *49,* 1277–1284.
5. M. Zanfir, A. Gavriilidis, Modeling of a catalytic plate reactor for dehydrogenation-combustion coupling. *Chem. Eng. Sci.,* **2001**, *56,* 2671–2683.
6. P. Häussinger, Ullmann's Encyclopedia of Industrial Chemistry. *Hydrogen,* 1989, Vol. A13, VCH Verlagsgesellschaft, Weinheim, 311 ff.
7. E. U. Schlünder, *Introduction into heat transfer,* Vieweg, Braunschweig, 3rd edn, 1981.
8. G. Kolios, B. Glöckler, A. Gritsch, et al., Heat-Integrated Reactor Concepts for Hydrogen Production by Methane Steam Reforming. *Accepted for Publication in Fuel Cells*. 2004.
9. G. Kolios, Zur autothermen Führung der Styrolsynthese mit periodischem Wechsel der Strömungsrichtung. *Nr. 501, VDI-Fortschrittsberichte, Reihe 3, VDI-Verlag, Düsseldorf,* 1997.
10. R. Charlesworth, A. Gough, C. Ramshaw, Combustion and steam reforming of methane on thin layer catalysts for use in catalytic plate reactors. *Fourth UK/National Conference on Heat Transfer, Institution of Mechanical Engineers, 26–27 September* 1995, pp. 85–89.
11. G. Kolios, J. Frauhammer, G. Eigenberger, Autothermal Fixed-Bed Reactor Concepts. *Chem. Eng. Sci.,* **2000**, *55,* 5945–5967.
12. R. F. Blanks, T. S. Wittrig, D. A. Peterson, Bidirectional adiabatic synthesis gas generator. *Chem. Eng. Sci.,* **1990**, *45,* 2407–2413.
13. A. M. De Groote, G. F. Froment, Synthesis Gas Production from Natural Gas in a Fixed-Bed Reactor with Reversed Flow. *Can. J. Chem. Eng.,* **1996**, *74,* 735–742.
14. K. Gosiewski, Simulations of non-stationary reactors for the catalytic conversion of methane to synthesis gas. *Chem. Eng. Sci.,* **2001**, *56,* 1501–1510.
15. G. Veser, J. Frauhammer, Modeling steady state and ignition during catalytic methane oxidation in a monolith reactor. *Chem. Eng. Sci.,* **2000**, *55,* 2271–2286.
16. R. G. Craig, T. J. Delaney, J. M. Duffalo, *Catalytic dehydrogenation performance of the catofin process*. DeWitt Petrochemical Review, Houston 1990.
17. C. Ercan, R. J. Gartside, Reactor Performance and Stability in an Alternating Reaction-Reheat Paraffin Dehydrogenation System. *Can. J. Chem. Eng.,* **1996**, *74,* 626–637.

18. T. N. Haynes, C. Georgakis, H. S. Caram, The application of reverse flow reactors to endothermic reactions. *Chem. Eng. Sci.,* **1992,** *47,* 2927–2932.

19. Yu. Sh. Matros, *Catalytic processes under unsteady-state conditions. Studies in surface science and catalysis.* 1989, vol. 43, Reversal of the reaction mixture flow in the fixed catalyst bed. Amsterdam: Elsevier.

20. O. Levenspiel, Chemical Engineer's Grand Adventure. *Chem. Eng. Sci.,* **1988,** *43,* 1427–1435.

21. M. S. Kulkarni, M. P. Duduković, A bidirectional fixed-bed reactor for coupling exothermic and endothermic reactions. *AIChE J.,* **1996,** *42,* 2897–2910.

22. M. S. Kulkarni, M. P. Duduković, Periodic operation of asymmetric bidirectional fixed-bed reactors with temperature limitations. *Ind. Eng. Chem. Res.,* **1998,** *37,* 770–781.

23. G. Kolios, G. Eigenberger, Styrene synthesis in a reverse-flow reactor. *Chem. Eng. Sci.,* **1999,** *54,* 2637–2646.

24. W. R. Humphries, E. I. Griggs, A design handbook for phase change thermal control and energy storage devices. *NASA Technical paper,* 1074, Washington DC, 1977.

25. B. Glöckler, G. Kolios, G. Eigenberger, Analysis of a novel reverse-flow reactor concept for autothermal methane steam reforming. *Chem. Eng. Sci.,* **2003,** *58,* 593–601.

26. B. Glöckler, A. Gritsch, A. Morillo, et al., Autothermal reactor concepts for endothermic fixed-bed reactions. *Chem. Eng. Res. Des.,* **2004,** *82* (A2), 148–159.

27. J. D. Snyder, B. Subramaniam, A novel flow strategy for ethylbenzene dehydrogenation in a packed-bed reactor. *Chem. Eng. Sci.,* **1994,** *49,* 5585–5601.

28. M. van Sint Annaland, *A novel reverse flow reactor coupling endothermic and exothermic reactions.* PhD thesis, Twente University, Enschede, The Netherlands, 2000.

29. U. Nieken, O. Watzenberger, Periodic operation of the Deacon process. *Chem. Eng. Sci.,* **1999,** *54,* 2619–2626.

30. A. Salden, *Adsorption/Incineration Process for Waste Gas Purification.* Ph.D. thesis, University of Stuttgart, Germany. 2002, Logos Verlag Berlin.

31. www.fuelcelltoday.com: Knowledge Bank.

32. E. H. Stitt, P. E. J. Abbott, B. J. Cromarty, et al., Emerging Trends in Syngas and Hydrogen. Presented at CatCon2000, 12–13 June, 2000, Houston, TX, USA.

33. E. H. Stitt, Multifunctional Reactors? 'Up to a Point Lord Copper'. *Chem. Eng. Res. Des.,* **2004,** *82* (A2), 129–139.

34. H. P. Schmidt, J. A. Wünning, FLOX· Steam Reforming for PEM Fuel Cell Systems. 59th "Congresso ATI", Genua, 2004.

35. J. Wünning, Flammenlose Oxidation von Brennstoff mit hochvorgewärmter Luft Chem.-Ing.-Tech., **1991,** *63,* 1243–1245.

36. A. Docter, G. Konrad, A. Lamm, Reformer für Benzin und benzinähnliche Kraftstoffe. *VDI – Berichte,* **2000,** *84,* 399–411.

37. S. Springmann, *Kinetische Grundlagen und dynamische Simulation der autothermen Kraftstoffreformierung.* PhD thesis, University of Stuttgart, Germany. 2003, Logos Verlag Berlin.

38. P. S. Chintawar, B. Bowers, C. O'Brien, et al., Advanced High Efficiency Quick Start Fuel Processor for Transportation Applications. *Progress Report for Hydrogen, Fuel Cells, and Infrastructure Technologies Program. U.S. Department of Energy;* 2003.

39. N. Edwards, S. R. Ellis, J. C. Frost, et al., On-board hydrogen generation for transport applications: the HotSpot• methanol processor. *J. Power Sources,* **1998,** *71,* 123–128.

40. M. Schuessler, M. Portscher, U. Limbeck, Monolithic integrated fuel processor for the conversion of liquid methanol. *Catalysis Today,* **2003,** *79–80,* 511–520.

41. M. Krumpelt, T. R. Krause, J. D. Carter, et al., Fuel processing for fuel cell systems in transportation and portable power applications. *Catalysis Today,* **2002,** *77,* 3–16.

42. S. Ahmed, R. Ahluwalia, S. H. D. Lee, Quick-Starting Fuel Processors – A Feasibility Study. *Progress Report for Hydrogen, Fuel Cells, and Infrastructure Technologies Program. U.S. Department of Energy;* 2003.

43. M. Zanfir, A. Gavriilidis, Catalytic combustion assisted methane steam reforming in a catalytic plate reactor. *Chem. Eng. Sci.,* **2003,** *58,* 3947–3960.

44. A. L. Dicks, S. L. Jones, R. Judd, et al., Assessment of advanced catalyst performance and fabrication options for a compact steam reformer. *Technical report: ETSU F/02/00180/REP, U.S. Department of Trade and Industry;* 2001.

45. J. Frauhammer, *Ein neues Gegenstrom-Reaktorkonzept für endotherme Hochtemperaturreaktionen.* PhD thesis, University of Stuttgart, Germany. 2003, VDI Verlag, Düsseldorf.

46. G. Kolios, J. Frauhammer, G. Eigenberger, A simplified procedure for the optimal design of autothermal reactors for endothermic high-temperature reactions. *Chem. Eng. Sci.,* **2001,** *56,* 351–357.

47. Z. R. Ismagilov, V. V. Pushkarev, O. Yu. Podyacheva, et al., A catalytic heat-exchanging tubular reactor for combining of high-temperature exothermic and endothermic reactions. *Chem. Eng J.,* **2001**, *82,* 355–360.

48. F. A. Robbins, H. Zhu, G. S. Jackson, Transient modeling of combined catalytic combustion/CH_4 steam reforming. *Catalysis Today,* **2003,** *83,* 141–156.

49. A. Gritsch, G. Kolios, G. Eigenberger, Reaktorkonzepte zur autothermen Führung endothermer Hochtemperaturreaktionen. *Chem.-Ing.-Tech.,* **2004,** *76,* 722–725.

50. G. Kolios, J. Frauhammer, G. Eigenberger, Efficient reactor concepts for coupling of endothermic and exothermic reactions. *Chem. Eng. Sci.,* **2002,** *57,* 1505–1510.

51. G. Friedrich, G. Gaiser, G. Eigenberger, et al., *Kompakter Reaktor für katalytische Reaktionen mit integriertem Wärmerücktausch.* European Patent, EP 0 885 653 B1, 2003.

52. V. A. Kirillov, N. A. Kuzin, A. V. Kulikov, et al., Thermally coupled catalytic reactor for steam reforming of methane and liquid hydrocarbons. *Theor. Found. Chem. Eng.,* **2003,** *37,* 1–9.

53. A. Morillo, A. Freund, C. Merten, Concept and design of a novel compact reactor for autothermal steam reforming with integrated evaporation and CO cleanup. *Ind. Eng. Chem. Res.,* **2004,** *43,* 4624–4634.

54. R. Killpack, Ullmann's Encyclopedia of Industrial Chemistry. Propene, 1989, Vol. A22, VCH Verlagsgesellschaft, Weinheim, 217 ff.